frontiers in Built Environment

TECHNOLOGY REPORT
published: 22 November 2018
doi: 10.3389/fbuil.2018.00066

Multi-Scale Remote Sensing of Tornado Effects

J. Arn Womble[1,2]*, *Richard L. Wood*[3] *and Mohammad Ebrahim Mohammadi*[3]

[1] School of Engineering, Computer Science, and Mathematics, West Texas A&M University, Canyon, TX, United States, [2] Insurance Institute for Business and Home Safety, Richburg, SC, United States, [3] Department of Civil Engineering, University of Nebraska–Lincoln, Lincoln, NE, United States

To achieve risk-based engineered structural designs that provide safety for life and property from tornadoes, sufficient knowledge of tornado wind speeds and wind flow characteristics is needed. Currently, sufficient understanding of the magnitude, frequency, and velocity structure of tornado winds remain elusive. Direct measurements of tornado winds are rare and nearly impossible to acquire, and the pursuit of *in situ* wind measurements can be precarious, dangerous, and even necessitating the development of safer and more reliable means to understand tornado actions. Remote-sensing technologies including satellite, aerial, lidar, and photogrammetric platforms, have demonstrated an ever-increasing efficiency for collecting, storing, organizing, and communicating tornado hazards information at a multitude of geospatial scales. Current remote-sensing technologies enable wind-engineering researchers to examine tornado effects on the built environment at various spatial scales ranging from the overall path to the neighborhood, building, and ultimately member and/or connection level. Each spatial resolution contains a unique set of challenges for efficiency, ease, and cost of data acquisition and dissemination, as well as contributions to the body of knowledge that help engineers and atmospheric scientists better understand tornado wind speeds. This paper examines the use of remote sensing technologies at four scales in recent tornado investigations, demonstrating the challenges of data collection and processing at each level as well as the utility of the information gleaned from each level in advancing the understanding of tornado effects.

Keywords: tornado damage, damage assessment, imagery, lidar, UAS, SAR, photogrammetry

OPEN ACCESS

Edited by:
Matthew Mason,
The University of Queensland, Australia

Reviewed by:
David Brett Roueche,
Auburn University, United States
Radhika Sudha,
Birla Institute of Technology and Science, India

***Correspondence:**
J. Arn Womble
awomble@ibhs.org

Specialty section:
This article was submitted to Wind Engineering and Science, a section of the journal Frontiers in Built Environment

Received: *16 May 2018*
Accepted: *16 October 2018*
Published: *22 November 2018*

Citation:
Womble JA, Wood RL and Mohammadi ME (2018) Multi-Scale Remote Sensing of Tornado Effects. Front. Built Environ. 4:66. doi: 10.3389/fbuil.2018.00066

INTRODUCTION

Tornadoes are the most violent of all atmospheric storms and rank among the most destructive and feared of natural hazards. Although they are known to produce some of the strongest winds on earth, a sufficient understanding of the magnitude, frequency, and velocity structure of tornado winds continues to elude researchers (Edwards et al., 2013). Direct measurements of tornado winds are extremely rare, difficult, and dangerous to obtain, largely due to the damaging and unpredictable nature of tornadoes and limitations on predicting tornado occurrences and paths (Fleming et al., 2013; Karstens et al., 2013; Kosiba and Wurman, 2013). Tragically, this has resulted in several injuries and deaths of experienced storm chasers in the pursuit of direct observations and measurements of tornadoes (Wurman et al., 2014). Direct measurement of tornado winds are further complicated by the inability of radar systems (including mobile systems) to measure the tornado winds near the ground surface, the location that most often impacts the built environment

(Wurman et al., 2013; Lombardo et al., 2015a; LaDue et al., 2017). As a result, in the absence of direct wind speed measurements, the detailed study of tornado effects on the natural and built environments has necessarily become essential for gaining critical insight into estimated tornado wind speeds, occurrence and geographical distribution, and tornado-structure interactions.

Improved understanding of tornado wind speeds and tornado-induced loads on structures is primarily reliant on the study of actual tornado damage (Kikitsu and Sarkar, 2015; Huang et al., 2016). A heightened understanding of tornado frequency and intensity is also necessary to establish climatologies to create risk-based engineering design philosophies and insurance underwriting. In this approach, the detection of tornado tracks in sparsely populated areas (i.e., based on damage signatures rather than direct observation by tornado spotters) is critical to the establishment of accurate tornado climatologies and occurrence intervals. However, damage investigations in rural areas (where structures are infrequent) are challenging due to the lack of damage indicators. Studies of treefall patterns and vegetation scour have helped to improve estimates tornado intensity and near-ground wind (Fujita, 1989; Bech et al., 2009; Beck and Dotzek, 2010; Karstens et al., 2013; Wakimoto et al., 2016).

The Enhanced Fujita (EF) Scale of tornado intensity aims to correlate observed levels of damage with wind speed ranges (TTU, 2006). Currently, these wind speeds are based on *estimates* derived from an expert-elicitation process (McDonald et al., 2009). Although the EF Scale serves as the official metric of tornado intensity for the U.S. and Canada, the wind speeds currently employed in the scale have not been verified, and their accuracy has been often debated. This is due to the estimation of tornado intensity as based on observed damage requires some knowledge of structural responses under wind loads (Doswell et al., 2009; Prevatt et al., 2012b; Edwards et al., 2013; Fratinardo and Schroeder, 2013). Data validation and corrections of EF Scale wind speeds are crucial for accurately predicting wind speeds necessary to achieve safe and economical structural designs as well as equitable insurance loss models. Such modifications depend on the forensic analysis of buildings, trees, and other damage indicators.

Emerging remote-sensing technologies, including satellite, and aerial imaging, and lidar, have demonstrated a constantly increasing efficiency for collecting, archiving, organizing, and communicating hazards information at numerous geospatial scales (Eguchi et al., 2008; Pittore et al., 2016). The capture of three-dimensional (3D) condition data, accomplished as quickly as possible after a tornado touchdown, can provide crucial and perishable evidence for detailed forensic damage assessments (e.g., Prevatt et al., 2011, 2012a,b, 2013; Smith et al., 2012; van Derostyne et al., 2012; Walsh and Tezak, 2012; Roueche and Prevatt, 2013; van de Lindt et al., 2013; Standohar-Alfano and van de Lindt, 2016). Detailed forensic studies of tornado damage assists researchers in understanding tornado-structure interaction; however, such studies require accurate measurements of member sizes and deformations, which can difficult to obtain in the field due to limited site access, safety, available field time, and the perishable nature of critical damage evidence (e.g., clean-up, post-storm water damage). Remote sensing imaging technologies have also proven effective for detecting and delineating tornado tracks in remote areas, particularly forested areas that may otherwise go undetected due to a lack of population and trained spotters (e.g., Skow and Cogil, 2017). Recent analysis techniques have also shown promise for estimating the intensity of tornadoes in forested areas (e.g., Jedlovec et al., 2006; Molthan et al., 2011, 2014; Karstens et al., 2013; Godfrey and Peterson, 2017).

BRIEF HISTORY OF REMOTE SENSING OF WIND DAMAGE AT MULTIPLE SPATIAL SCALES

The remote sensing analysis of wind effects on the built environment has advanced through the study of tornado damage and other windstorms, including thunderstorms, downbursts, and hurricanes. Although precise wind load mechanisms causing damage to individual structures can vary significantly between tornadoes and other windstorms, the *techniques,* which includes remote-sensing technologies, for the study of damage are quite similar for multiple types of windstorms; thus, the study of damage from hurricanes and other types of wind storms is also beneficial to the advancement of remote-sensing analysis of tornado damage.

Remote sensing for observation of tornado effects can be traced to the middle of the twentieth century (Skow and Cogil, 2017). The U.S. National Weather service has employed aerial observations and aerial photography in the surveying of tornado tracks and tornado damage from the 1950s to the present (van Tassel, 1955; Wakimoto et al., 2016). Aerial imaging and observations played a particularly significant role in the seminal tornado research of Dr. Theodore Fujita starting in the mid-1960s (McDonald, 2001; Yuan et al., 2002). Such aerial surveys, however, required knowledge of tornado occurrence and location to schedule or charter aerial flights.

As technology advanced, detection and study of tornado tracks with earth-observing satellite (EOS) data became possible with the launch of the Landsat-series satellites starting in the early 1970s. Early images from the 1970s captured still-visible tracks of multiple tornadoes that had occurred earlier (most likely in 1965) in forested areas of South America (Dyer, 1988; Jedlovec et al., 2006). Since the 1990s, the use of high-resolution multi-spectral satellite imagery has significantly enhanced the ability to detect tornado tracks (Jedlovec et al., 2006). One notable example is the analysis of the 1999 Oklahoma City Tornado Outbreak and its various tracks using digital remote-sensing analysis techniques including principal component analysis (PCA) and normalized difference vegetation index (NDVI) (Yuan et al., 2002).

The modern era of remote sensing for the assessment of wind damage to individual structures can be traced to the launch of the first high-resolution (sub-meter) commercial satellite in 1999, following deregulation of the industry by the U.S. government. Womble et al. (2007a) conducted a seminal study using 60-cm

commercial satellite and 35-cm NOAA aerial images to wind damage assessment following Hurricanes Charley and Ivan in 2004. Womble et al. (2006) also explored the utility of 21 satellite and aerial remote-sensing platforms (spatial resolutions ranging from 30 cm to 5 km) for gauging the impact of *hurricane* damage at numerous geospatial levels, resulting in a tiered *Remote-Sensing Reconnaissance System* (**Figure 1**) for assessment of wind damage in Hurricane Katrina (2005) at levels ranging from *regional* (Tier 1), to *neighborhood* (Tier 2), and *per-building* (Tier 3). From 1999 to 2016, the finest-possible spatial resolution of commercial satellite imagery has improved by more than three-fold, from 100 cm (IKONOS) to 31 cm (WorldView 4).

Aerial Imaging Platforms

Aerial imaging platforms have the potential of providing data more quickly than earth-orbiting satellite platforms, as these platforms are not subject to the limitations of imaging time windows and revisit times, which may coincide with cloud cover. Aerial platforms also can acquire multiple view angles of the same areas. Hurricane Katrina (2005) saw the advent of widespread acquisitions of pre- and post-storm aerial imagery using the Pictometry fleet of more than 70 light aircraft to provide five view angles (vertical/nadir and 4 oblique/off-nadir angles) with 15-cm spatial resolutions at three spectral bands in the visible range (red, green, and blue). For the next decade, per-building (Tier 3) analyses facilitated highly-detailed remote sensing assessments for hurricane and tornado damage via satellite and aerial imagery (e.g., Womble et al., 2010, 2016; ImageCat/New Light Technologies, 2011; Brown et al., 2012; Atkins et al., 2014; Gong and Maher, 2014; Luo et al., 2014a; Ortega et al., 2014).

The U.S. mainland experienced nearly a decade-long respite from major hurricane landfalls between Hurricane Ike (2008) and Hurricane Harvey (2017). However, during this time, the U.S. experienced several severe tornado outbreaks, including Super Tuesday (2009), Birmingham-Tuscaloosa, AL (2011), Joplin, MO (2011), Moore, OK (2013), Pilger, NE (2014), and Pampa, TX (2017). Major advances in the remote sensing of wind effects thus progressed primarily through the study of *tornado* damage during this period, particularly through the advent of accessible 3D lidar (light detection and ranging or laser) scanning, photogrammetry, and unmanned aerial systems (UAS) for detailed preservation of damage conditions at the sub-centimeter level (Prevatt et al., 2011, 2013; Graettinger et al., 2012, 2014; Kashani and Graettinger, 2015; Kashani et al., 2015, 2016; Wood and Mohammadi, 2015; Womble et al., 2016). These most recent developments have significantly demonstrated enhanced remote-sensing capacities by adding an additional tier, Tier 4 (**Figure 1**), which includes a resolution that facilitates analysis at the *member–connection level* enabling highly detailed forensic investigations of wind-induced structural failures. These data sets can be retained after the evidence is removed by repair or demolition efforts. The 2017 hurricane season brought major hurricanes Harvey, Irma, and Maria to North America, all of which are destined to bring further advances in the remote-sensing analysis of wind-damaged structures, which can, in turn, advance the analysis of tornado damage.

TORNADO PATH LEVEL (TIER 1)

Need for Improved Tornado Climatology Information in Sparsely Populated Areas

An accurate understanding of tornado risks for a region (based on historical records of tornado occurrences, intensity, and path extents) is essential to achieve safe and economical engineering designs and more equitable insurance underwriting. Historic records of tornado occurrences, path extents, and intensities have historically been limited to real-time observations of the tornadoes themselves and/or investigation of damage to damage indicators (such as structures or trees). Specific to tornado occurrences in sparsely populated areas, such occurrences are likely to go unobserved due to lack of damage indicators, leading to inaccurate tornado climatologies based on incomplete historical data. Consequently, to more accurately define the tornado climatology, there is a need for detection and estimation of tornado intensity in sparely populated areas where tornado occurrences may otherwise go undetected. Tornadoes occurring in open prairie or plains areas may or may not leave noticeable traces, depending largely on types of ground cover, species of agricultural crops, and crop maturity stage within the season (Skow and Cogil, 2017). Tornadoes occurring in forested areas, however, typically leave distinguishable evidence in the form of widespread tree damage.

Establishing Improved Tornado Climatologies

Establishing improved tornado climatologies requires both (1) *detection* and (2) *determination of the intensity* of tornadoes. In the absence of both direct wind speed measurements and observable damage, the gauging of tornado intensities based on effects on *natural forested environments* has received notable attention (Peterson, 2003, 2007; Frelich and Ostuno, 2012; Karstens et al., 2013; Lombardo et al., 2015b; Cannon et al., 2016; Godfrey and Peterson, 2017). Remote-sensing imagery, including satellite and/ or aerial imaging and lidar capabilities (Darnell, 2012) provides an effective basis for the confirmation of tornadoes in forested and low-population areas where tornadoes may otherwise go undetected. Broad-scale geospatial data, as from earth-observing satellites (EOS), can verify the occurrence (tracks) of suspected tornadoes and can provide pertinent information about path locations, lengths, and widths (Bentley et al., 2002; Yuan et al., 2002; Myint et al., 2008; Molthan et al., 2011, 2014), thereby providing a basis for more accurately developing the tornado climatology of a region.

"Missing" Tornadoes in Remote Forested Areas

Comprehensive records of tornado occurrences have been maintained in the U.S. since the 1950s and in Canada since the 1980s (Etkin et al., 2001). These records are based on observations of tornadoes or damage paths and often are not acquired at all in sparsely populated areas. Undercounting of tornadoes significantly affects the accuracy of regional tornado climatologies (Doswell and Burgess, 1988) and leads to erroneous assessment of risks to life and property (Brooks, 2013; Lloyd's of

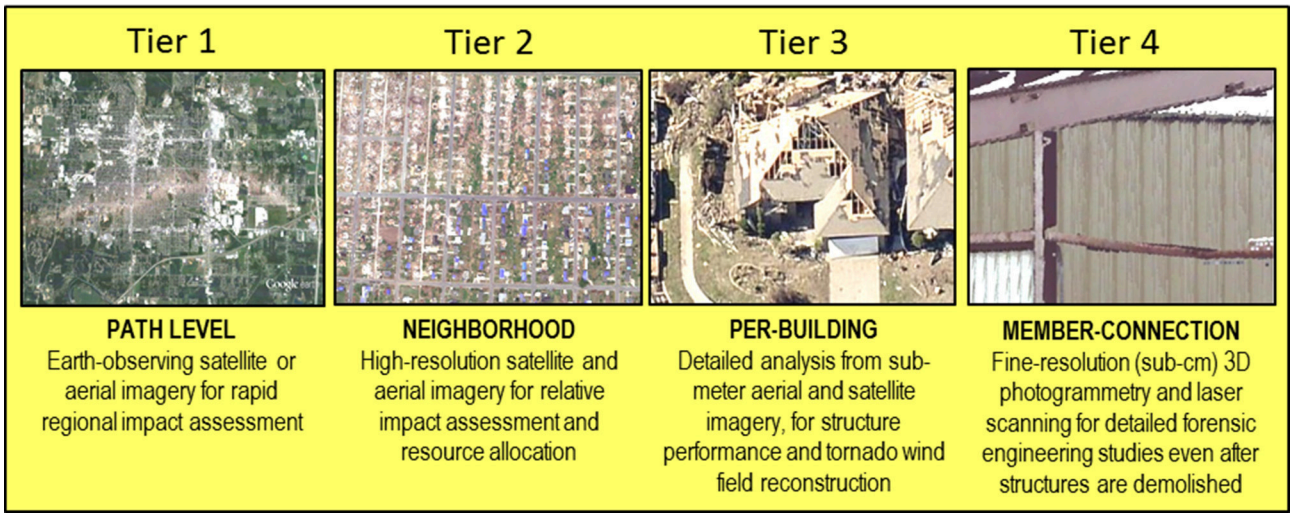

FIGURE 1 | Four distinct tiers for remote sensing of tornado effects at different spatial levels. Image credit: Google, NOAA (public domain), and authors.

London, 2013). Low population density has long been credited as a primary factor in the failure to observe tornadoes (Snider, 1977; Schaefer and Galway, 1982; Anderson et al., 2007; Cheng et al., 2013, 2015). Studies of tornado climates of sparsely populated areas of Ontario (Sills, 2012; Sills et al., 2012; Cheng et al., 2013), using integrated lightning flash density and population density data, suggest that at least 50% of tornadoes in Canada's sparsely populated areas may go undetected; in particular, they expose a suspected population bias resulting in "missing" tornadoes for an extensive region of southwest Ontario due to its rural landscape.

Tornado Path Analysis With Earth-Observing Satellite Data

Earth-observing satellite (EOS) imagery plays a significant role in the detection and geolocation of overall tornado occurrences and paths. Collected data have several different geospatial resolutions and revisit times (imaging frequencies), including NASA's MODIS sensors (250 m resolution; daily revisit), ASTER sensor (15 m; daily-on demand), and Landsat Enhanced Thematic Mapper (ETM) sensors (30 m; 16-day revisit). For example, **Figure 2** shows the track of the June 1, 2011, EF3 tornado that struck Sturbridge, MA in 30-m natural-color imagery acquired by the Landsat 5 Thematic Mapper sensor on June 5, 2011.

With larger spatial resolutions corresponding to the coarser EOS imagery (30–250 m), visual inspection alone is often not sufficient for the detection of tornado tracks. Enhancements to EOS visual imagery are helpful for the detection of tornado tracks (i.e., disturbed vegetation in forested areas). Example methods include PCA using proper orthogonal decomposition of digital images, and NDVI) analysis accomplished by mathematically combining red-visible and near-infrared wavelength reflectance values, which correspond to vegetation health within each pixel (**Figure 3**). Early investigations with EOS imagery addressed the detection of tornado paths (Jedlovec et al., 2006). The 1999 Oklahoma City, OK, tornado outbreak provided an opportunity for several significant studies of tornado path detection using EOS data. Magsig et al. (2000) and Yuan et al. (2002) applied PCA techniques and NDVI imagery derived from the Indian Remote Sensing satellite to detect tornado tracks (**Figure 4**). Myint et al. (2008) employed Landsat-TM imagery from the same tornado outbreak in a comparison of image processing techniques (including PCA and object- detection-based approaches) for the detection of tornado tracks.

More recently, researchers applied PCA and NDVI methodologies in preliminary studies to help determine tornado intensity in forested areas of Alabama using NASA EOS imagery following the April 2011 tornado outbreak, with specific emphasis to provide immediate guidance for ground surveys (Molthan et al., 2011, 2014). NDVI enhancements using post-tornado images alone were helpful for semi-automated detection of paths for strong tornadoes; however, before-and-after images were necessary to identify paths of weaker tornadoes (Molthan et al., 2014). For 30-m Landsat imagery of the 2011 tornado outbreak in forested areas of Alabama, Kingfield and deBeurs (2014) observed that a Disturbance Index derived from 6 Landsat spectral bands more consistently identified severe tornado paths than did an NDVI analysis derived from 2 spectral bands. Analysis parameters needed for producing beneficial results (helpful for the identification of tornado tracks) were found to be highly dependent on the specific vegetation of a region, strongly indicating that additional explorations are necessary to yield beneficial results for tornadoes in other geographic and climatic areas.

Tornado Path Analysis With Synthetic Aperture Radar (SAR) Data

Active remote sensing systems, such as synthetic aperture radar (SAR) systems, transmit a signal and measure a return (e.g., backscatter from the surface), unlike passive optical sensors which measure reflectance and temperature. Such active remote

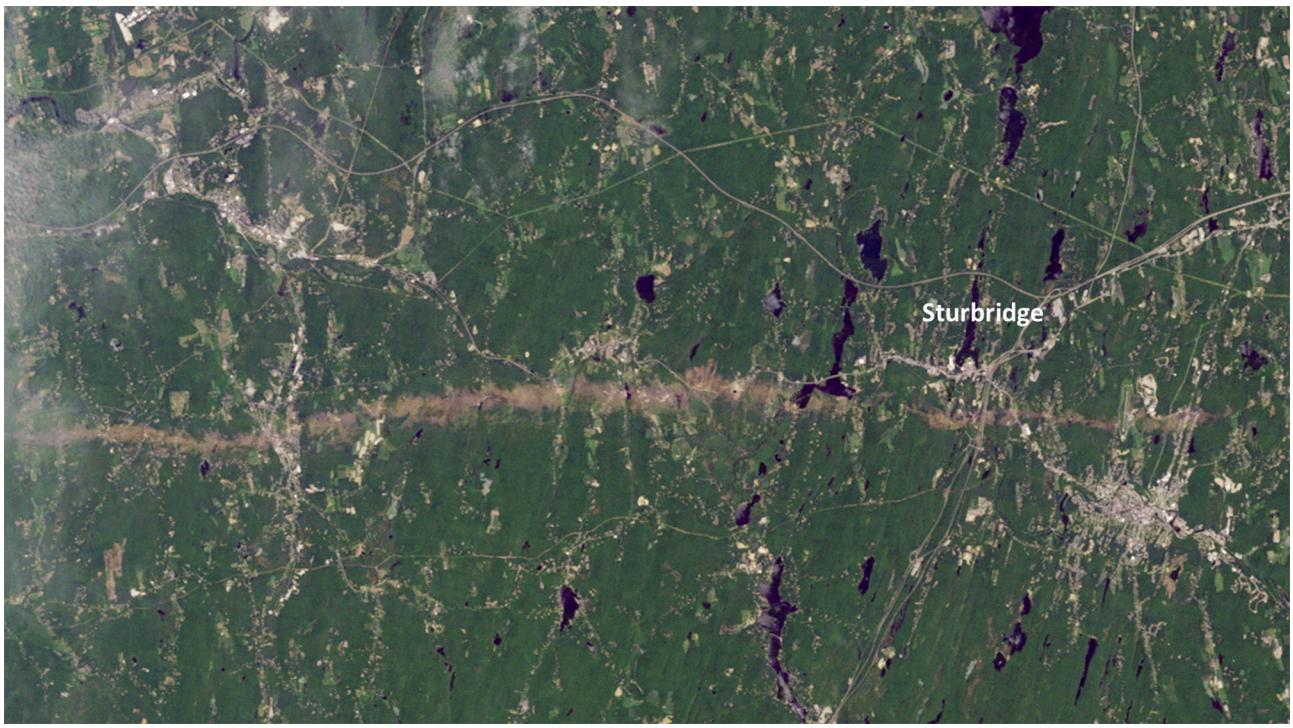

FIGURE 2 | Natural color image (30 m) from Landsat 5 Thematic Mapper showing tornado track from June 1, 2011. The town of Sturbridge, MA, was struck by this EF3 tornado. Image acquired on June 5, 2011. Image credit: NASA (public domain).

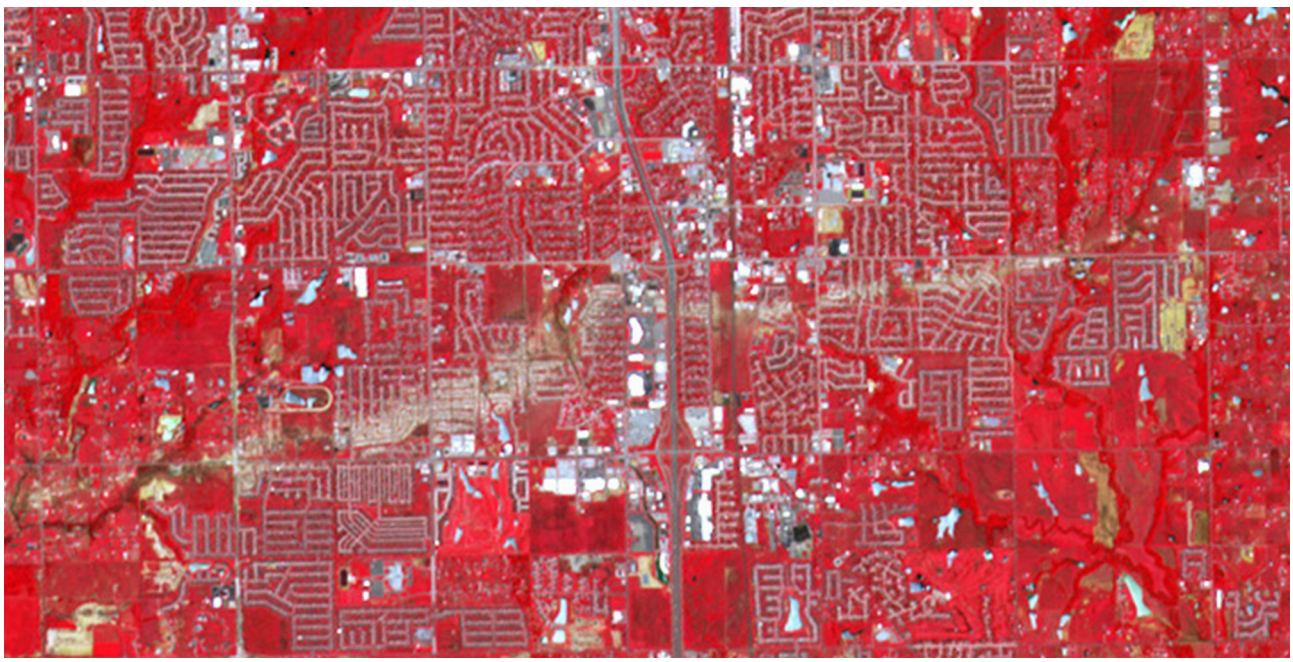

FIGURE 3 | Track of the EF-5 tornado that struck Moore, OK, on May 20, 2013 is visible in the false-color image composed of infrared, red, and green bands acquired by the Advanced Spaceborne Thermal Emission and Reflection Radiometer (ASTER) on board NASA's Terra satellite on June 2, 2013. In this false-color image, vegetation appears as red, and the tornado track (absence of vegetation) is clearly evident. Spatial resolution 15 m. Image credit: NASA (public domain).

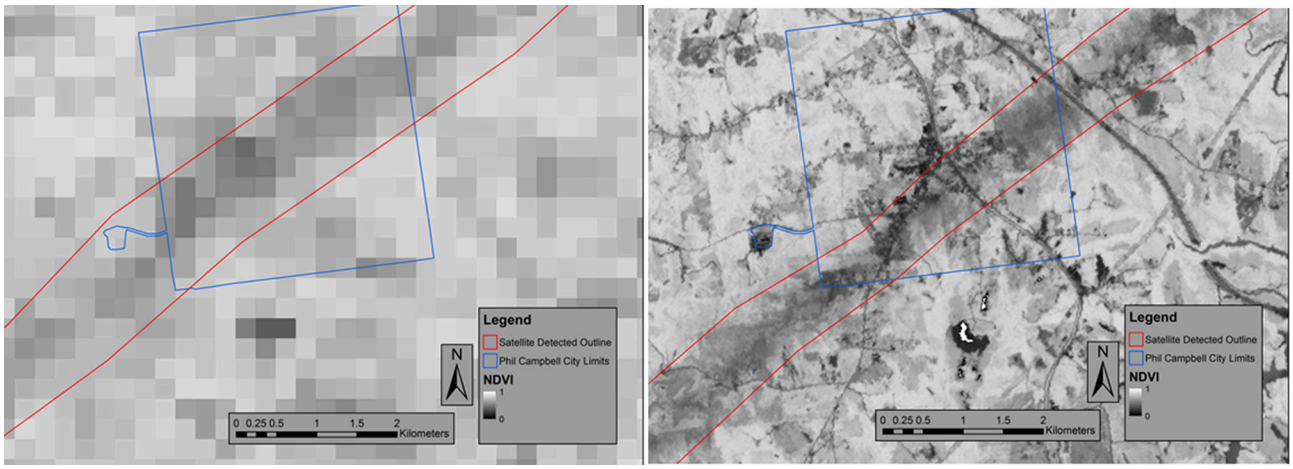

FIGURE 4 | Tornado track of April 27, 2011 near Phil Campbell, AL, is visible in NDVI imagery from Terra MODIS (250 m, May 4, 2011) and Terra ASTER (15 m, May 20, 2011). Image Credit: Andrew Molthan, NASA SPoRT (public domain).

sensing systems can be used in any light condition (day or night) and with any sky conditions (cloud cover), giving them greater versatility for imaging by not being hindered by daylight or cloud-free conditions. Schultz (2016, 2017) describes NASA SPoRT's use of SAR tornado imagery in the U.S. National Weather Service's Damage Assessment Toolkit (DAT) to facilitate the identification of damage tracks in areas where damage surveys are especially challenging, such as densely forested areas and areas with limited road access. **Figure 5** shows a SAR change-detection (multitemporal) image obtained by subtracting SAR return values from before-and-after images of a 2017 tornado in a heavily forested area near Clear Lake, WI.

Tornado Path Analysis With High-Resolution Aerial Data

The relatively coarse resolution of EOS data does not enable the viewing of individual structures or trees; however, aerial platforms offer much higher spatial resolutions for imagery but require specific tasking for data acquisition and thus some prior knowledge of the existence and (approximate) location of tornado tracks.

Vertical aerial imagery collected by NOAA (25 cm) provided the basis for several different studies of tornado effects in the severe 2011 Joplin, MO, and Tuscaloosa-Birmingham, AL, tornadoes (**Figure 6**). For example, Karstens et al. (2013) employed the NOAA 25-cm aerial imagery to analyze treefall patterns in a study of the near-ground wind fields for the 2011 Joplin, MO tornado. Cannon et al. (2016) and Godfrey and Peterson (2017) also used high-resolution (20-cm) aerial imagery for estimation of tornado intensity and mapping of local tornado wind fields based on visually identified treefall patterns in remote or inaccessible forest areas in the southeastern U.S.

Oblique aerial imagery (often obtained by hand-held camera systems in light aircraft) is also effective in showing overall tornado paths. For instance, the path of the 2013 EF5 tornado at Moore, OK, is readily evident in the oblique imagery of **Figure 7**.

Automated Urban Tornado Path Detection

Significant advancements in automated tornado path detection in urban areas based on monotemporal (post-event only) aerial and satellite images of various spatial resolutions are reported by Radhika et al. (2012). The automated path detection is based on a texture-wavelet analysis of deposition patterns of tornado debris, which is most commonly encountered in urban settings. These investigations utilized high-resolution (0.1 m) aerial imagery for the 2006 Saroma (Japan) tornado, moderate (1-m) resolution commercial satellite imagery for the 2003 Moore, OK, tornado, and coarse (30-m) satellite imagery for the Tuscaloosa, AL tornado of 2011. These investigations highlight the importance of improved spatial resolutions for more accurately estimating the tornado path width.

NEIGHBORHOOD LEVEL (TIER 2)

Use of Neighborhood Data (Wind Feld Analysis)

Detailed analysis of damage patterns throughout a neighborhood region can enhance the understanding of tornado wind fields, including both the intensity and low-level structures of tornado circulations (Fujita, 1981; Luo et al., 2014b; Wakimoto et al., 2016). Highly detailed neighborhood-level data is useful for fragility analysis of residential structures (Roueche and Prevatt, 2013; Roueche et al., 2015; Kopp et al., 2017). High-resolution (sub-meter) satellite imagery and aerial imagery are commonly used for such analyses. Regional damage assessments can be accomplished either at the regional level (typically for automated assessments) or as an amalgamation of per-building (Tier 3) damage data with the use of either semi-automated or visual assessments. **Figure 8** shows an example of the 25-cm

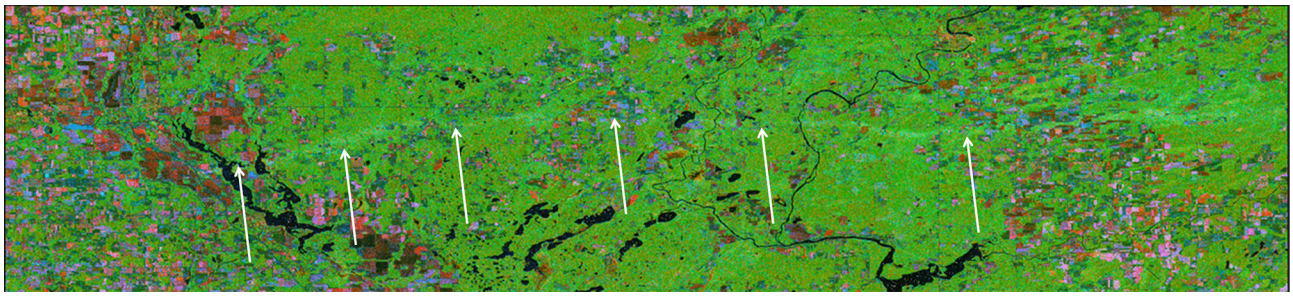

FIGURE 5 | Synthetic Aperture Radar (SAR) temporal difference image (before-and-after) of the tornado track from May 16, 2017 near Clear Lake, WI. Imagery acquired by Sentinel-1(A/B), a European Space Agency (ESA) satellite with a SAR instrument on board. The above image is the result of differencing images from May 10 and May 22, 2017. Image credit: Lori Schultz, NASA SPoRT (public domain).

FIGURE 6 | Photomosaic image (created from multiple NOAA 25-cm aerial images) showing path of 2011 Joplin, MO tornado. Image Credit: NOAA (public domain).

neighborhood-level aerial imagery acquired by NOAA alongside pre-event imagery for a neighborhood affected by the 2011 Tuscaloosa, AL, tornado.

Need for Visual Damage Assessment

Despite the now-widespread availability of satellite and aerial imagery following major disasters, damage assessment using remote-sensing imagery is still heavily reliant on visual assessment (Ghosh et al., 2011). This is due to the slow progress in robust and automated damage assessment algorithms. Until algorithms for automated damage assessments have reached a mature level, practical applications for rapid damage assessments across large areas necessarily employ visual screening based on remote-sensing imagery (Womble et al., 2010; Atkins et al., 2014). Because of the current necessity of using rapid visual assessment of first-available data, recent research has targeted the accuracy of visual assessments made with imagery of various spatial resolutions (Brown et al., 2012; Luo et al., 2014a,b).

Case Study—Tuscaloosa and Joplin Tornadoes (2011) (Amalgamation of Per-Building Data)

ImageCat, Inc. and New Light Technologies completed a rapid building damage assessment after the extremely destructive tornado outbreaks in Tuscaloosa, AL, and Joplin, MO, using the 25-cm NOAA aerial imagery sets described above in an

FIGURE 7 | Oblique photo from hand-held camera system in light aircraft clearly show the path of the 2013 EF5 tornado at Moore, OK. After: Dr. Nolan Atkins, Lyndon State University, NSF RAPID Response Grant AGS-1343963 (public domain: http://meteorology.lyndonstate.edu/vortex2/Moore2013/).

evaluation of the efficacy of remote-sensing technologies for rapid post-disaster damage assessment (Womble et al., 2016). This study focused on levels of damage that are discernible from remotely-sensed imagery and the speed at which these results could be delivered to personnel in the field. In the development of this description, FEMA's 4-point Tornado Damage scale was used along with the Enhanced Fujita (EF) Scale and a remote-sensing-based damage scale (Womble, 2005; Womble et al., 2007b). This work was transformative in that observable information from aerial surveys was merged with expert engineering knowledge regarding the behavior of buildings subjected to extreme winds to arrive at an integrated, remote-sensing-based damage scale. This investigation demonstrated the importance of pre-event imagery in assessing post-event damage levels, as it was essential to understand the pre-event geometry of each structure to assign a final damage level. Assessment of damage levels was difficult when very high-resolution aerial imagery (pre-event) was unavailable. Another key result of the damage analysis was the identification of damaged buildings by occupancy (residential or commercial). This information was important in supporting the housing assistance program and in identifying the owners of damaged buildings, accomplished by linking tax assessor's parcel information to the locations of damaged buildings. Damage to some building surfaces (walls, windows, and doors) could not be directly observed from vertical remote-sensing imagery, the methodology was shown to provide nearly 100% accuracy for detection catastrophic damage (structures were completely destroyed) given that very high-resolution pre-event imagery (of ~25 cm or finer) is available for baseline comparison.

Figure 9 shows the distribution of damaged buildings in the 2011 Joplin, MO, tornado obtained as an amalgamation of per-building damage assessments. More than 8,000 buildings were

FIGURE 8 | Before-and-after imagery of neighborhood in Tuscaloosa, AL, struck by tornado on April 27, 2011. Left image credit: Google Earth. Right image: 25-cm aerial imagery. Image credit: NOAA (public domain).

identified as having some level of damage. Finally, to improve the overall damage assessment operations using remotely-sensed data, a set of recommendations for response to future events was identified, including availability of high-resolution vertical and oblique aerial data before and after any event, creation of pre-event planning databases (such as parcel boundaries with occupancy, structural type, etc. information), establishing methods to quantify accuracy and confidence levels of the damage assessment, and expanding the knowledge of damage assessment for tornadoes to other hazards.

Unmanned Aircraft Systems

Satellite and aerial imagery can cover large areas; however, such data may not be available, economical, or practical for relatively small or isolated tornado or other windstorm events. Much earth-observing satellite data can also be too coarse to assist with detailed damage assessments at the neighborhood- or per-building level (Tiers 2 and 3, respectively). In such instances, ground-based data acquisition techniques have often been employed. For instance, vehicle-mounted cameras have also been used to rapidly acquire data throughout affected areas (Womble et al., 2006; Luo et al., 2014a,b); however, these systems can be severely limited in their ability to view all external surfaces of affected buildings, as side views can be obscured by nearby structures, and rear views may be inaccessible altogether. Obstacles such as trees, fences, and other vehicles can also occlude direct views of building surfaces. Access to affected neighborhoods may also be restricted or prohibited by law-enforcement operations, natural roadblocks (e.g., fallen trees or flooded roadways), private-property concerns, or other dangerous conditions (e.g., structures in danger of imminent collapse). In such cases, observation from above the roof height is often beneficial.

Notable recent advancements in unmanned aircraft systems (UAS) have made the use of such systems quite viable for the collection of highly-detailed damage information from above roof levels at the neighborhood- and per-building scales. UAS platforms also offer the ability to remotely view and capture damage conditions in real-time. Miller (2017) describes the utility of UAS technology for emergency response for the May 2017 EF-2 tornado that struck Elk City, OK (Miller, 2017). With knowledge of likelihood of tornadoes in the nearby area, a team was positioned just miles away when the tornado struck. Within 20 min of the tornado's strike, the team deployed a quadcopter which streamed live video to the state Emergency Operations Center in Oklahoma City (120 miles away) as well as the National Weather Service office in Norman, OK. Officials from these organizations were able to direct the data acquisition in real-time by requesting flights over certain areas and identify locations for detailed views of specific structures.

Mobile Lidar

One of the newer and most efficient ways to rapidly deploy a lidar platform is through mobile lidar systems (MLS). Although MLS requires sizeable capital investment, it can collect data from large areas rapidly. MLS platforms consist of one or multiple lidar scanners and a series of cameras to collect color information as well as an inertial measurement unit (IMU) and a GPS sensor. The ground sampling distance (GSD) within MLS data is dependent on the specific equipment and on the travel speed during the data collection. The GSD of the collected data can vary between 30 to 3 cm for a travel speed of 16 to 80 kph using mapping-grade and surveying grade MLS platforms, respectively (Gong, 2014). As a result, MLS platforms can scan large areas in short timeframes and create a detailed and accurate point clouds along with corresponding color information, intensity return values, and accurate locations. However, the survey process can be limited by multiple factors including loss of GPS signal (due to urban canyons), occlusion (due to vegetation, automobiles and debris), prohibited access to damaged areas (due to road closures), access to limited surfaces (only capturing the roadway sides of a structure), and lighting conditions (affecting the RGB color information). Recently, Gong (2014) investigated the application of the MLS-derived point clouds for post disaster geospatial data collection within New York and New Jersey following Hurricane Sandy. To assess the damage sustained by structures after the event, Gong (2014) used scan data collected pre- and post-hurricane to perform a change detection analysis to identify damaged areas, partially collapsed buildings, and structural displacement/movement.

BUILDING LEVEL (TIER 3)

Overview

A relatively large amount of research and development concerning tornado effects on the built environment has focused on the per-building level, including single-family residences and commercial/ industrial buildings. This is defined herein as Tier 3, where the individual building level is a logical level for assessment for several practical reasons, including insurance underwriting and adjustment and detailed forensic studies. It is consistent with the rating of tornado intensity by the Enhanced Fujita scale (TTU, 2006) as a Damage Indicator (such as Single-Family residences FR12), and this forms a natural level of detail for visual assessments. The per-building level also forms a logical basis for automated assessments via computer algorithms as groups of contiguous pixels (representing individual structures) serve as the basis for numerous automated damage studies (e.g., Thomas et al., 2012, 2014; Kashani and Graettinger, 2015; Kashani et al., 2015). For purposes of insurance risk and resiliency, damage functions (fragility curves) are also commonly constructed at the

FIGURE 9 | Per-building analysis of damaged buildings in Joplin, MO (2011). Image Credit: ImageCat (used with permission).

per-building level (Roueche and Prevatt, 2013; van de Lindt et al., 2013; Roueche et al., 2015; Kashani et al., 2016; Masoomi and van de Lindt, 2016; Kopp et al., 2017).

Building Types

Attention has primarily focused on large, simple-form industrial buildings (especially in the development of semi-automated damage detection algorithms, e.g., Thomas et al., 2012, 2014) and on single-family residences. Single-family residences constitute the most populous category of buildings sustaining damage in major windstorms. For instance, a comprehensive city-wide investigation of damage incurred by the 2011 Joplin, MO, tornado showed that residential structures comprised ∼94% of the nearly 8000 damaged structures (NIST, 2014b). Womble (2005) and Womble et al. (2007a) demonstrated that single-family residences present significantly more complicated geometric forms than other types of buildings, and that finer spatial resolutions are required to accurately determine the damage levels for such complex building forms than for simple building forms (e.g., larger rectangular warehouse buildings).

Use of Building-Level Data for Understanding Tornado Effects

Early estimates of tornado loads on buildings were based on horizontal, straight-line boundary layer winds; however, atmospheric measurements (e.g., Lee and Wurman, 2005; Karstens et al., 2010; Kosiba and Wurman, 2010) and physical models (e.g., Mishra et al., 2008; Sengupta et al., 2008; Hu et al., 2011; Yang et al., 2011; Prevatt et al., 2013) confirm that the vertical velocity components are significantly larger in tornadoes. Physical modeling efforts further suggest that tornado-induced building pressures can be several times greater than non-tornado wind pressures specified by current load standards (e.g., Mishra et al., 2008; Haan et al., 2010). Haan et al. (2014) emphasize the need for field investigations and preservation of data sets to provide validation and calibration for physical simulations of tornadoes. Comprehensive and accessible damage data are likewise beneficial for the validation of tornado risk models (Masoomi and van de Lindt, 2016; Peng et al., 2016; Standohar-Alfano and van de Lindt, 2016), load models (Thampi et al., 2011; Roueche et al., 2015; Koliou et al., 2017) and new building code wind provisions (Ramseyer et al., 2016). The study of tornado damage to buildings is of particular importance to the estimation of tornado intensity, as building structures constitute a majority of damage indicators (DIs) in the Enhanced Fujita Scale (currently 23 of 28 DIs are building structures).

Case Study: Moore, OK

The Moore, Oklahoma, EF-5 tornado of 2013 damaged over 4,000 structures, producing a full range of damage levels (EF-0 to EF-5) to residential structures (Ortega et al., 2014). Pictometry International (now EagleView Technologies) collected over 20,000 aerial (nadir and oblique) images of the affected area during the 2 days immediately following the tornado. This survey covered an area of 123 square miles and included vertical and oblique images of each property (PropertyCasualty360, 2013). Atkins et al. (2014) collected over 1,100 aerial photographs with a digital single-lens reflex camera from a Cessna 172 aircraft 2 days after the tornado. Atkins' team assigned EF-Scale damage values to more than 4,000 structures using the National Weather Service EF Kit (LaDue and Mahoney, 2006) and compared their dataset of EF-Scale values for consistency with an independent ground survey of the Moore tornado conducted by teams affiliated with the U.S. National Weather Service (Burgess et al., 2014).

Low-Level Aerial Imaging

Low-level aerial surveys can also prove advantageous for building-level (and city-block sized) surveys, particularly for small, non-major events of interest (where NOAA aerial imaging may not be deployed) and/or where access is limited or restricted. The authors commissioned the Aerial Oklahoma Corporation to obtain low-level (5-cm) aerial images of major buildings at

FIGURE 10 | Low-level (5-cm) aerial imagery of metal building structures damaged by the EF-3 tornado at the Halliburton Oilfield Services facility outside Pampa, TX, in November 2015. (Image Credit: Authors/Aerial Oklahoma Inc.).

the Halliburton industrial facility that was severely damaged by an EF-3 tornado in November 2015. Due to safety and liability concerns, the property managers restricted site access; however, the authors were permitted to obtain damage information remotely (from overhead and/or aerial platforms and from the fence lines). **Figure 10** shows an example of 5-cm imagery for individual buildings at the Halliburton facility. The image resolution is sufficiently fine to observe global failure patterns for overall structures and even for some larger structural members.

Unmanned Aircraft Systems (Per-Building Scale)

Adams et al. (2014) detail the recent use of UASs for collection of building-level damage data for earthquakes, hurricanes, and tornadoes. Of particular interest here is the case study of the use of a UAS platform to obtain sub-centimeter still images as well as video imagery [from a height of ∼20 m above ground level (AGL)] for damage to structures from the 2012 EF-3 tornado in Athens and Harvest, AL. Through the use of a UAS platform and the resulting imagery, the research team was able to identify specific construction materials, building condition, failure mechanisms, and even failure sequences for specific structures. Womble et al. (2016) utilized UAS platforms to view additional buildings at the Halliburton facility; the UAS was particularly helpful for viewing the interior of the building shown in **Figure 11** at an altitude of ∼80 feet AGL. It revealed the presence of an overhead crane system within the building that gave the building additional lateral support, and therefore additional lateral wind resistance than would ordinarily be assumed by use of the metal building system damage indicator from the current Enhanced Fujita Scale.

Ground-Based Lidar

With the ability to supply sub-cm spatial resolutions, ground-based (also known as terrestrial or stationary) lidar (GBL) systems may be used to provide three-dimensional damage information at either the per-building level or the member/connection level. Given the time and expense required to obtain a set of scans (generally 4–6 or more scans with ∼8–15 min per scan), the present operational use of GBL appears to be most effective for the Tier 4 level rather than for determining damage at the per-building level. Investigations utilizing GBL for Tier 3-type analyses (e.g., Kashani et al., 2014, 2015, 2016; Kashani and Graettinger, 2015) demonstrate that lidar-based wind damage signatures can be *correlated* with wind speeds estimates from other (*independent*) sources, such as the EF Scale; in such applications, the lidar data are used to arrive at a general damage state without considering member damage at the Tier 4 level. It is notable that such correlations of damage states with independently determined wind speeds may also be similarly achieved with Tier 3 photographic images, as shown by Brown et al. (2012) and (Thomas et al., 2012, 2014); such damage states depend on the overall performance of a structure or portions of a structure and are not necessarily assessed based on member deflections (Tier 4).

Complementary Uses of Photogrammetry and Lidar for Point Cloud Analysis Techniques

Modern photogrammetry techniques offer the ability to produce point clouds from handheld digital cameras and UAS platforms with onboard cameras, with a distinct advantage being the much faster possibility for data acquisition as compared to GBL systems (minutes as opposed to hours). Zhou et al. (2016) examined mobile-platform digital photogrammetric (DPG) techniques and mobile lidar platforms and found that these mobile platforms facilitated damage assessments consistent with >1 cm pixel size (Tier 3). Lidar scanning equipment is relatively costly and requires more time for data acquisition; however, later processing of acquired lidar data into a 3D point cloud is relatively fast and straightforward. DPG requires relatively low-cost digital camera equipment and software, using an advanced computer vision technique known as Structure-from-Motion (SfM). DPG has found widespread use in vehicle and aircraft crashes (Jurkofsky, 2015; Osman and Tahar, 2016) and crime scene investigations (Buck et al., 2013); many such investigations are also now complementary with lidar scanners. Limited comparative studies indicate that DPG or SfM and lidar data

FIGURE 11 | UAS-based imagery of metal building structures damaged by the EF-3 tornado at the Halliburton Oilfield Services facility outside Pampa, TX, in November 2015. (Image Credit: R. L. Wood).

are, in general, complementary for common applications at the per-building (Tier 3) level (Stal et al., 2013; Gneeniss et al., 2015; Jurkofsky, 2015; Kedzierski and Fryskowska, 2015), though lidar may exhibit slightly better accuracy (Szabo et al., 2016) with less noise and thus may be most optimally used for limited collection of high-resolution data where sub-centimeter information (e.g., member deformations—Tier 4) are desired. While vehicle crashes and wind-damage investigations both require rapid evidence preservation, the spatial extent of the wind damage is typically far more immense (by orders of magnitude), highlighting the time required to collect evidence for each of numerous individual structures as well as the need to balance the breadth (DPG) and depth (lidar) of data-acquisition capabilities. DPG data acquisition is relatively quick and can be accomplished by static, walking, driving, or low-level aerial surveys. Data processing into the 3D point cloud requires more computational time, and overall results are expected to have slightly lower accuracy than ground-based lidar scanning for observing member sizes and deflections, making such data a good candidate wherever cm- (rather than mm-) level accuracy and resolution (e.g., GSD) is sufficient at Tier 3. To streamline the investigation of tornado-damaged structures enhanced by reality capture, optimized strategies for collecting pertinent data with these complementary platforms are required to achieve an optimal balance (depth vs. breadth) of damage evidence within Tier 4.

Semi-Automated Damage Assessments

In an operational capacity, remote-sensing-based damage assessments are presently pursued using a mixture of semi-automated algorithms visual assessments. Notable progress has been made in the pursuit of automated wind damage assessments for large, simple-form industrial buildings and single-family residences (the highest percent of structures). To date, semi-automated assessments of wind damage have been achieved in research applications, while operational damage assessment using remote-sensing imagery remains predominately reliant on visual assessments, as robust damage assessment algorithms have been slow in development and verification (Ghosh et al., 2011; Thomas et al., 2014; Womble et al., 2016).

Rapid assessment of damage requires the ability to utilize first-available imagery, which may encompass a variety of spatial and spectral resolutions. Automated change detection using before-and-after images from different platforms is aggravated by a lack of spatial correspondence in pixels; hence, comparisons of objects or features (pixel groups) are more effective than pixel-to-pixel comparisons (Womble et al., 2007b). In the early development of semi-automated damage assessment algorithms, Womble (2005) identified remote-sensing signatures of wind damage for the four most common building types: single-family residences, mobile homes, metal warehouses, and industrial buildings with built-up roofs; this study showed that wind damage has distinctly different remote-sensing characteristics depending on building type. For each type of building, progressive levels of wind damage were described from a remote-sensing perspective. Womble (2005) identified 4 distinct levels of damage for single-family residences discernable in aerial and satellite images and consequently formulated separate damage descriptions for each of the building types. Subsequent researchers (Brown et al., 2012; Luo et al., 2014a,b) have further refined these damage levels for single-family residences by subdividing these original damage levels into as many as 36 different levels. (Thomas et al., 2012, 2014) made additional strides toward automated remote-sensing wind damage assessment for simple rectangular (commercial) buildings damaged by hurricanes and the 2011 Joplin tornado using moderate resolution imagery (50 to 1 m). The resulting algorithms predicted damage with an overall accuracy of 72 to 80% for simple-form buildings (such as rectangular warehouses). Radhika et al. (2015) employed high-resolution, pre- and post-event satellite data for the estimation of percent damage to individual building structures, observing a correlation factor of 0.78 between automatically identified damage and manually (visually) identified damage.

Crowdsourcing and Citizen Science

In the absence of fully automated damage-assessment quantification algorithms, "crowdsourcing," (i.e., web-based rapid visual assessments by a large number of interested and semi-trained volunteers) provides a means of streamlining rapid damage assessments that can prove useful for the proposed project. Crowdsourcing was employed extensively for time-sensitive remote-sensing analysis of the 2010 Haiti earthquake (Ghosh et al., 2011; Bevington et al., 2015; Glasscoe et al., 2016)

and showed similar promise for use in wind-related disasters. Commercial satellite image providers also began providing open-access satellite imagery for areas affected by natural disasters such as Hurricanes Patricia (2015), Matthew (2016), and Harvey (2017), for use in organized crowdsourcing efforts such as the Tomnod Project (DigitalGlobe, 2017). It is anticipated that such crowdsourcing efforts will also help to streamline large-scale quantification of damage for major, widespread tornado events which can assist in damage assessments as well as advance the field of "citizen science" or "citizen engineering." (Potential drawbacks to citizen science and citizen engineering stem from the fact that may of the participants are only partially trained; as a result, damage metrics often utilize multiple detectors to eliminate false positives or erroneous selections).

MEMBER-CONNECTION LEVEL (TIER 4)

Overview

The most recent advances in remote-sensing technologies now enable the detection and analysis of damage, as well as the preservation of damage evidence, at the individual member-connection level via non-contact methods enabling measurements from a safe distance—especially helpful when access is prohibited, restricted, difficult, and/or dangerous. With sub-centimeter resolutions, these technologies facilitate the measurement of deflections for individual structural members and cladding panels. Such measurements are critical for the calibration and/or validation of structural analysis models aimed at the back-calculation of (estimated) tornado wind speeds based on damage to structures.

Lidar Technology

Lidar technology, an active remote sensing technique, has rapidly progressed and proven highly effective for the rapid collection of 3D scene-condition information from both mobile and stationary platforms. Terrestrial (stationary) 3D lidar (or laser) scanners provide the means to rapidly obtain accurate and measurements of structures from a distance, enabling investigators to obtain measurements of member sizes and deformations that would not otherwise be possible due to issues with safety, access, and time. Systems typically offer the added benefit of supplemental full-color imaging to colorize the 3D point cloud nodes for enhanced reality capture and visual identification. Lidar has seen notable applications in detailed analysis of earthquake and tsunami effects (Olsen et al., 2012; Chock et al., 2013; Brando et al., 2015; Wood and Mohammadi, 2015; Bose et al., 2016; He et al., 2016) as well as storm-surge actions (Hatzikyriakou et al., 2015). Lidar has also seen use in the collection of recent tornado and hurricane damage data (Prevatt et al., 2011, 2013; Graettinger et al., 2012; Wood and Mohammadi, 2015; Womble et al., 2016; Kijewski-Correa et al., 2018). Lidar provides copious amounts of 3D data for damaged structures but, at present, is relatively slow compared to other data-collection technologies; for optimal analysis of widespread damage. Consequently, it has been strategic to use lidar sparingly and strategically for carefully selected structures (for which detailed forensic analysis can yield higher quality information about tornado-induced loads) and to supplement data collection for other structures with other technologies. This is due to the time and planning required to collect lidar point clouds of structures.

Unmanned Aerial/SfM Systems

One of the newer platforms for the remote sensing of wind damage include unmanned aerial vehicles (UAV) with payloads of digital and/or still cameras (making these into unmanned aerial systems—UAS). UASs offer a number of distinct advantages for the rapid acquisition of high-resolution damage information for windstorms and other hazards over large areas including mountainous terrains and urban centers (Moss et al., 2015; Bose et al., 2016). UASs are available in a variety of grades and user levels—ranging from the amateur/hobby level to the commercial (near-survey-grade, real-time kinematics) level. Early use of UASs in earthquake-damaged areas (Brando et al., 2015; Wood and Mohammadi, 2015; Bose et al., 2016) has proven the utility of UASs for damage data collection. UASs are well-equipped for rapidly capturing wind damage data, as they offer the advantage of overhead imaging at various altitudes and with user-controlled imaging angles (nadir and off-nadir). Overhead imaging has been found to be particularly well-suited for detection and assessment of damage due to wind action, and thus offer viewing angles generally superior to those which are available for ground-based investigations (Womble et al., 2007a). UASs also offer the advantage of user-configurable flight controls from manual to fully-autonomous missions. "Remote pilots" (operators) can direct a UAS in real time and observe conditions of structures at extremely close range to the object or areas of interest—from positions and view angles not otherwise available due to accessibility or safety concerns (Murphy, 2015). UASs also are well-suited for following linear tornado paths as they can be controlled manually in real-time for exploratory investigations of specific damage sites or pre-programmed to follow specific autonomous flight plans, e.g., Miller, 2017. However, UASs are unable to acquire data in high-wind conditions, and short battery life can also provide obstacles for extended uses; the extents of the limitations are specific to the selected UAS platforms. UAS platforms are also well-suited as a cost-effective substitute to aerial lidar platforms, using photogrammetric approaches to construct 3D point clouds using a series of 2D images through SfM algorithm (as detailed in section Complementary Uses Of Photogrammetry and Lidar For Point Cloud Analysis Techniques).

Unlike satellite imaging platforms, the application of UAS platforms requires operators to travel to damage areas. However, UAS platforms are less-limited by revisit times and atmospheric conditions such as cloud cover and haze than are satellite-imaging platforms. UASs can therefore collect data more rapidly provided that investigators are able to travel quickly to the damage site. UASs can also provide much finer spatial resolution for detailed damage assessments, with sub-centimeter ground sampling distances or pixel spacing. Given the proper circumstances, UAS systems can often provide first-available and highly-detailed damage information, e.g., Miller, 2017, although legal and operational issues can hinder the timeliness

of UAS-based acquisitions, as under the governance of the Federal Aviation Administration (FAA) and other local agencies. Commercial UAS flights in the U.S. are presently limited to uncontrolled airspace, but permission is improving with the FAA adoption of the Low Altitude Authorization and Notification Capability (LAANC). Rapidly changing government restrictions on the legal operation of UASs, e.g., requirements for pilot certification of commercial UASs, restrictions on flight altitudes, and line-of-sight (LoS) operations, may create some of the primary hindrances to the most-efficient use of UASs for such data acquisitions, e.g., beyond line of sight (BLoS).

Emphasis on Damage to Simple Engineered Structures

Investigation of damage to simple engineered structures is of particular interest, since the resistance of simple structures can often be estimated, helping researchers to more fully understand the load mechanisms producing failures (Lloyd's of London, 2013). Such determination requires accurate measurement of structural member sizes, which can be prohibitive due to time, site access, and safety issues. Lidar and UAS geospatial data is particularly well-suited to provide highly detailed forensic studies of individual structural members, thereby leading to wind speed estimates that can provide much-needed updates (or validations) for the EF Scale.

Joplin, MO, Tornado Case Study (2011)

The 2011 Joplin, MO tornado damaged more than 8,000 residences. Tornado damage forced evacuation and demolition of the St. John's Regional Medical Center. Close inspection and measurements were impractical due to its size and prohibitions on site access, so inspection teams utilized ground-based lidar scanning to rapidly obtain high-precision geometric data for subsequent detailed forensic studies (Prevatt et al., 2013). The resulting 3D point cloud enabled determination of elevations, distances, lengths, and deformations, which could not otherwise be rapidly or directly measured. Graettinger et al. (2012) also employed lidar scanning to rapidly capture post-storm condition data for residential buildings, institutional structures, terrain features, and trees. In each case, lidar scanning was able to obtain measurements that could not otherwise be obtained due to accessibility constraints and time limitations.

Pilger, NE Tornado Case Study (2014)

A severe weather system in the U.S. Great Plains on June 16 to 19, 2014 produced more than 100 tornadoes, including two EF-4 tornadoes near the small town of Pilger, NE. The historic Wisner-Pilger Middle School was severely damaged (**Figure 12**). Wood and Mohammadi (2015) deployed stationary terrestrial lidar and a tethered UAV with an onboard camera to characterize the damage to the exterior of the school. The lidar scanning directly produced a 3D point cloud, while the UAS images required further processing via SfM to reconstruct the scene as a 3D point cloud. Using point clouds, the geometry and textural details were captured, thereby enabling non-destructive evaluation of potential damage (Wood and Mohammadi, 2015). For this building, 11 exterior lidar scans and multiple UAS passes were conducted to acquire 844 2D images for the SfM algorithm that yielded a point cloud with sub-centimeter level details. **Figure 12** illustrates the resultant point cloud of the Wisner-Pilger Middle School that is useful for future engineering analysis and assessment. For this study, the performance of two different roof systems was assessed. The light-gauge truss roof section experienced a 50% failure rate compared to a failure rate for rolled-steel W-section roof supports of only 6%.

Pampa, TX Tornado Case Study (2015)

An intense tornado outbreak produced at least 17 tornadoes stretching across portions of the Texas Panhandle, Oklahoma, and Kansas on November 16 and 17, 2015. The most intense of these tornadoes (EF-3) severely damaged a group of engineered structures at the Halliburton Oilfield Services facility near Pampa, TX (**Figure 13**). The Halliburton facility contained numerous types of engineered structures for which structural resistances could be estimated, thereby enabling the estimation of tornado wind speeds required to cause the observed damage. The tornado also overturned nearby engineered center-pivot irrigation (CPI) systems (**Figure 14**), which are common to many rural and tornado-prone areas of the U.S. For safety and security concerns, owners of the Halliburton facility made immediate plans to demolish the damaged buildings and restricted all access to the site; investigators were thus not able to make direct contact measurements of structural member sizes and deformations to permit resistance calculations. Engineering researchers (Womble et al., 2016, 2017a,b; Mohammadi et al., 2017) were able to utilize stationary terrestrial lidar and UAS platforms to acquire 3D data of damaged structures from the property line. Primary structural steel members of the pre-engineered metal buildings were visible, so measurements of the member sizes could be utilized in structural analysis models to validate or correct the wind speed estimates for damage to pre-engineered buildings in the current EF Scale. Lidar scanning as well as aerial imaging and UAS imaging provided effective solutions for rapidly and accurately preserving damage data for subsequent detailed forensic analysis.

Although direct access to the nearby CPI system was possible, measurements of the overall structure (∼350 m) and deformations were most readily accomplished by lidar scanning and UAS imaging. Scanning of this structure introduced a unique challenge due to its length and geometry. Unlike typical infrastructure-type structures (e.g., bridges and buildings), the CPI structure does not have large or wide members. The structure's length and the lack of wide surfaces and shapes, made the scanning plan and registration process particularly challenging due to a non-closed traverse scan strategy. To achieve this task, a total of six 225 mm diameter retro-reflective sphere targets were used within the 12 scans at a spacing of 35 m. The CPI was scanned at distances of roughly 10 m with similar scan settings to that of Halliburton facility, resulting in a point cloud with an average point-to-point spacing of 1 cm. The resultant point cloud contained ∼800 k points. The sphere targets were used for an initial target-based registration which was later refined using a cloud-to-cloud optimization process. The final registration had a mean registration error of 21 mm.

FIGURE 12 | Tornado damage to Wisner-Pilger Middle School: ground-survey image **(Left)** and point-cloud imagery derived from lidar and SfM **(Right)**, located at Pilger, NE. (Image Credit: R. L. Wood/M. E. Ebrahim Mohammadi).

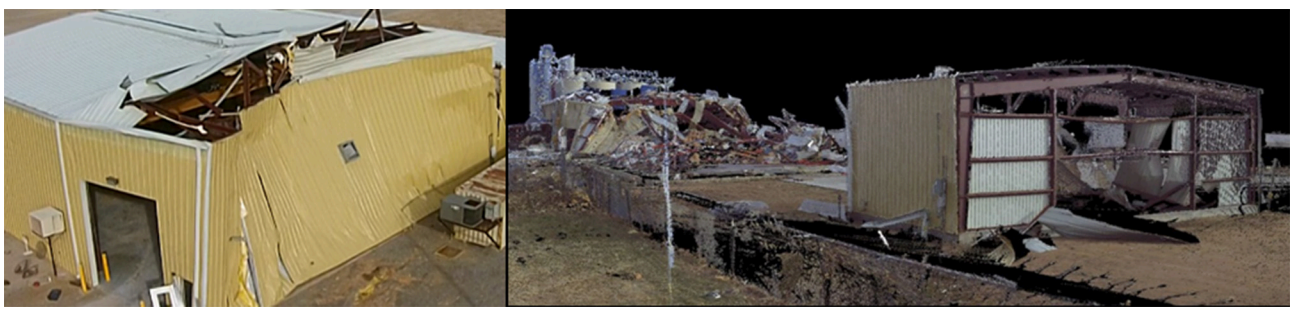

FIGURE 13 | UAS imagery **(Left)** and lidar point-cloud data of damaged Halliburton facility at Pampa, TX **(Right)**. (Image Credit: R. L. Wood/M. E. Ebrahim Mohammadi).

DISCUSSION AND RECOMMENDATIONS

Optimal Use of Sensors

Present-day tornado damage researchers are now equipped with an immense and ever-expanding array of remote-sensing-based platforms that enable them to rapidly and thoroughly obtain and preserve damage conditions for detailed forensic studies. Such studies can assist with the estimation of tornado wind speeds and with gaining a better understanding of near-ground tornado wind velocity and pressure distributions. There is an overlap between sensors and the various levels of their applications. A challenge is most effectively matching the sensor to the needs and objectives for data acquisition, to best leverage equipment costs, data collection times, and spatial resolutions for the information that is required. **Table 1** presents recommendations for optimal use of various sensors according to the desired spatial scales. With a view toward optimizing data collection in the wake of a tornado by balancing time, equipment, personnel, and financial resources, assessment of damage across a wide area may be accomplished with satellite or aerial imagery, which can be

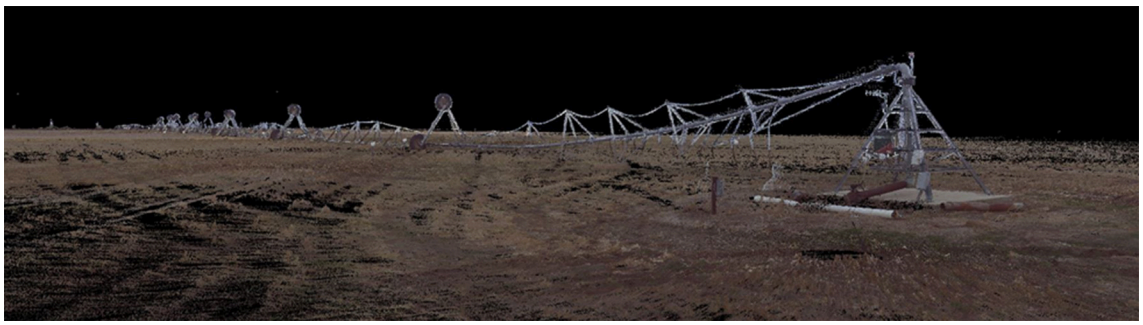

FIGURE 14 | Lidar point-cloud data for overturned center-pivot irrigation system at Pampa, TX. (Image Credit: R. L. Wood/M. E. Ebrahim Mohammadi).

collected more rapidly and across a much larger area to give a broader view of relative damage states. For instance, Prevatt et al. (2011, 2013) describe an effective and comprehensive strategy for field investigation of damage resulting from the severe (EF 5) tornado outbreaks of 2011 in Tuscaloosa, AL, and Joplin, MO. Investigators implemented a sampling strategy with an existing three-tier approach leveraging data acquisition speeds with various levels of detail, utilizing highly-detailed lidar-scanning data for engineered buildings where damage and failure mechanisms were of particular interest and where direct measurements of member sizes and deformations were not physically or practically possible. Particular attention should also be given to the relatively newly available stationary terrestrial lidar platform. The precision and detail offered by Tier 4 finds perhaps its most optimal niche in the detailed modeling of tornado failures at the member-deformation (sub-centimeter or even millimeter level): in emphasizing depth rather than breadth of damage (highly detailed damage for a few selected structures rather than more general damage levels for structures throughout a larger area). Due to relatively long scan times required to canvass an affected area with Tier 4 data as opposed to Tier 3 data, Tier 4 data are best reserved for strategically selected structures, for which detailed forensic analysis can yield higher quality information about tornado-structure interaction and induced loads.

TABLE 1 | Recommended optimal use of sensors by spatial scale.

Spatial scale	Recommendation for optimal sensor(s)
Tier 1 (Tornado Path)	Earth-Observing Satellites
	Aerial
Tier 2 (Neighborhood)	Aerial
	UAS
	Commercial Satellites (sub-meter)
	Mobile lidar
Tier 3 (Per-Building)	UAS
	Aerial (especially oblique)
	Commercial Satellites
	Digital Photogrammetry
	Mobile lidar (some views limited)
Tier 4 (Member/Connection)	Lidar
	UAS
	Digital Photogrammetry

Remote Sensing Data for Enhanced Understanding of Tornado Effects

The rapid preservation of detailed and perishable tornado-damage scenes enables researchers to advance the understanding of tornado effects by validating damage prediction models via physical modeling, computer modeling, and other predictive damage modeling (e.g., loss estimation and risk assessment models). The optimal use of available sensors minimizes collection times, costs, and efforts and also facilitates forensic structural engineering investigations, whenever access is limited. Data concerning the behavior of structures subjected to tornado loads are valuable to engineers, atmospheric scientists, and wind-hazard researchers, because the performance of these structures under the extreme tornado-induced loads help to validate (and/or correct) the wind speed estimates for the EF Scale. Due to the scarcity of direct measurements, the EF Scale has thus necessarily relied upon wind speeds estimates based on common damage indicators (e.g., trees, signs, light poles, and buildings). The majority of these damage indicators are situated in urban or forested areas, while damage indicators in rural areas remain scarce. For accurate populating of the national tornado database (necessary for risk assessments for engineering design and insurance modeling), it is necessary to obtain intensity information for all tornadoes: including urban and rural settings. Damage information for new damage indicators can be obtained using the above-mentioned platforms.

Remote Sensing in the Development of Tornado Wind Speed Standards

The inclusion of tornado effects in design standards currently varies throughout the world, understandably due to limited knowledge concerning near-ground tornado wind speeds and tornado-structure interactions. Guidance for tornado effects now lags far behind the guidance for hurricane effects in wind loading standards. The 2011 National Building Code of

Canada has made significant forward strides in the inclusion of tornado effects based on historical records and statistical projections (Sills, 2012; Sills et al., 2012). Although tornado load effects are not yet formally addressed in U.S. wind load and governing design code standards, Huang et al. (2016) describe a path for eventual inclusion of tornado loads in building code design: the process integrates the study of comprehensive tornado wind fields using atmospheric observations, numerical and physical simulations of tornado wind fields, and detailed structural analysis. NIST (2014a) recommends the continued exploration of remote-sensing technologies for post-storm damage investigations and field measurements to help validate windborne debris models as part of a comprehensive plan to change the current state of engineering practice to "improve life safety, reduce property damage, and improve the resiliency and sustainability of communities." Insurance industry leaders (Lloyd's of London, 2013) further emphasize the need for detailed studies of tornado damage to engineered structures to more fully understand the load mechanisms producing failures. The thorough preservation and detailed analysis of such damage is of particular significance given the relatively rare instances of tornadoes striking engineered structures compared to residential structures.

Remote-sensing technologies at a variety of geospatial scales offer various means for advancing the development of tornado wind load standards, including the improvement of regional tornado climatology for risk analysis by more thoroughly capturing all tornado occurrences (Tier 1), the advanced understanding of ground-level tornado wind fields (Tier 2), and an improved understanding of tornado-structure interactions and tornado wind speeds (Tiers 2–4).

An active joint effort of the American Society of Civil Engineers Structural Engineering Institute, the American National Standards Institute, and the U.S. National Weather Service seeks to significantly improve the accuracy of tornado wind estimates and the Enhanced Fujita (EF) Scale through the forthcoming ASCE Standard for Tornado Wind Speed Estimation (Lombardo et al., 2015a). Remote sensing of damage and the archiving of data for future analyses have received detailed and methodical attention since 2004, as new technologies and algorithms have become available (Womble et al., 2016) and play a critical role in the new ASCE standard. The Remote Sensing Subcommittee (of which authors JAW and RLW are leaders) is responsible for establishing accepted practices for assessment of damage to individual Damage Indicators and determination of tornado tracks using remote-sensing technologies.

AUTHOR CONTRIBUTIONS

JW oversaw the overall document with particular attention to discussion of Tiers 1, 2, and 3. RW contributed to the overall document and particularly to the discussions of Tier 2 and 4. MM aided in the preparation of **Figures 11–14**, overall text proofreads, and contributions to of Tier 2.

FUNDING

Partial funding for research efforts described herein has been provided by National Science Foundation Awards 1623553, 1626480, 1760010, and 1751018 at WTAMU, 1623542 at UNL, and 1623752 at TTU. Additional support was provided by the WTAMU Killgore Research Center, the University of Nebraska Foundation, and the University of Western Ontario (Northern Tornadoes Project).

ACKNOWLEDGMENTS

The authors are grateful for the assistance of Profs. Doug Smith and Elizabeth Louden (TTU Natl. Wind Institute), Ms. Lori Schultz and Dr. Andrew Molthan (NASA SPoRT), Dr. Darrel Kingfield (NOAA/ Univ. Colorado), Mr. Ron Eguchi and Mr. Shubharoop Ghosh (ImageCat, Inc.), WTAMU engineering students Brandon Bugarin, Vitor Patriani-Cardoso, Peter Hughes, and Rusty Johnston, the Halliburton Corporation, Wisner-Pilger School District, and operations division of the Nebraska Dept. of Transportation.

REFERENCES

Adams, S. M., Levitan, M. L., and Friedland, C. J. (2014). High resolution imagery collection for post-disaster studies utilizing unmanned aircraft systems (UAS). *Photogram. Eng. Remote Sens.* 12, 1161–1168. doi: 10.14358/PERS.80.12.1161

Anderson, C. J., Wikle, C. K., Zhou, Q., and Royle, J. A. (2007). Population influences on tornado reports in the United States. *Weather Forecast.* 22, 571–579. doi: 10.1175/WAF997.1

Atkins, N. T., Butler, K. M., Flynn, K. R., and Wakimoto, R. M. (2014). An integrated damage, visual, and radar analysis of the 2013 Moore, Oklahoma, EF5 tornado. *Bull. Am. Meteorol. Soc.* 95, 1549–1561. doi: 10.1175/BAMS-D-14-00033.1

Bech, J., Gaya, M., Aran, M., Figuerola, F., Amaro, J., and Arus, J. (2009). Tornado damage analysis of a forest area using site survey observations, radar data and a simple analytical vortex model. *Atmos. Res.* 93, 118–130. doi: 10.1016/j.atmosres.2008.10.016

Beck, V., and Dotzek, N., (2010). Reconstruction of near-surface tornado wind fields from forest damage. *J. Appl. Meteorol. Climatol.* 49, 1517–1537. doi: 10.1175/2010JAMC2254.1

Bentley, M. L., Mote, T., and Thebpanya, P., (2002). Using Landsat to identify thunderstorm damage in agricultural regions. *Bull. Am. Meteorol. Soc.* 83, 363–376. doi: 10.1175/1520-0477-83.3.363

Bevington, J., Eguchi, R., Gill, S., Ghosh, S., and Huyck, C. (2015). *A* "Comprehensive Analysis of Building Damage in the 2010 Haiti Earthquake Using High-Resolution Imagery and Crowdsourcing," in *Time-Sensitive Remote Sensing,* eds C. Lippitt, D. Stow, and L. Coulter (New York, NY: Springer), 31–145.

Bose, S., Nozari, A., Mohammadi, M. E., Stavridis, A., Moaveni, B., Wood, R. L., et al. (2016). "Structural assessment of a school building in Sankhu, Nepal damaged due to torsional response during the 2015 Gorkha earthquake," in *IMAC XXXIV A Conf. & Expo. on Structural Dynamics* (Orlando, FL), 25–28. doi: 10.1007/978-3-319-29751-4_5

Brando, G., Rapone, D., Spacone, E., Barbosa, A., Olsen, M., Gillins, D., et al. (2015). *Reconnasiance Report on the 2015 Gorka Earthqauke Effects in Nepal.* Associazione Nazionale Italiana di Ingegneria Sismica XVO Convegno (L'Aquila), 20.

Brooks, H. E. (2013). Severe thunderstorms and climate change. *Atmos. Res.* 123, 129–138. doi: 10.1016/j.atmosres.2012.04.002

Brown, T. M., Liang, D., and Womble, J. A. (2012). Predicting ground-based damage states from remote-sensing imagery. *J. Wind Struct.* 15, 369–383. doi: 10.12989/was.2012.15.5.369

Buck, U., Naether, S., Räss, B., Jackowski, C., and Thali, M. (2013). Accident or homicide - Virtual crime scene reconstruction using 3D methods. *Forensic Sci. Int.* 225, 75–84. doi: 10.1016/j.forsciint.2012.05.015

Burgess, D., Ortega, K., Stumpf, G., Garfield, C., Marshall, T. P., Meyer, T. C., et al. (2014). 20 May 2013 Moore, Oklahoma, Tornado: damage survey and analysis. *Weather Forecast.* 29, 1229–1237. doi: 10.1175/WAF-D-14-00039.1

Cannon, J. B., Hepinstall-Cymerman, J., Godfrey, C. M., and Peterson, C. J. (2016). Landscape-scale patterns of forest tornado damage in mountainous terrain. *Landsc. Ecol.* 31, 2097–2114. doi: 10.1007/s10980-016-0384-8

Cheng, V. Y. S., Arhonditsis, G. B. D., Sills, M. L., Auld, H., Shepherd, M. W., and Klaassen, J. (2013). Probability of tornado occurrence across Canada. *J. Clim.* 26, 9415–9428. doi: 10.1175/JCLI-D-13-00093.1

Cheng, V. Y. S., Arhonditsis, G. B. D., Sills, M. L., Gough, W. A., and Auld, H. (2015). A Bayesian modelling framework for tornado occurrences in North America. *Nat. Commun.* 6:6599. doi: 10.1038/ncomms7599

Chock, G., Carden, L., Robertson, I., Olsen, M., and Yu, G. (2013). Tohoku tsunami-induced building failure analysis with implications for U. S. tsunami and seismic design codes. *Earthquake Spectra* 29, S99–S126. doi: 10.1193/1.4000113

Darnell, C. (2012). *LiDAR Supports Advanced Geospatial Analysis.* Earth Imaging Journal. Available online at: http://eijournal.com/print/articles/lidar-supports-advanced-geospatial-analysis

DigitalGlobe (2017). *Hurricane Harvey Response.* Available online at: http://blog.digitalglobe.com/news/hurricane-harvey-response/ (Accessed December 29, 2017).

Doswell, C. A., Brooks, H. E., and Dotzek, N. (2009). On the implementation of the enhanced Fujita scale in the USA. *Atmos. Res.* 93, 554–563. doi: 10.1016/j.atmosres.2008.11.003

Doswell, C. A. III., and Burgess, D. W. (1988). On some issues of United States climatology. *Monthly Weather Rev.* 116, 495–501.

Dyer, R. C. (1988). Remote sensing identification of tornado tracks in Argentina, Brazil, and Paraguay. *Photogram. Eng. Remote Sens.* 54, 1429–1435.

Edwards, R., LaDue, J. G., Ferree, J. T., Scharfenberg, K., Maier, C., and Coulbourne, W. L. (2013). Tornado intensity estimation: past, present, and future. *Bull. Am. Meterol. Soc.* 94, 641–653. doi: 10.1175/BAMS-D-11-00006.1

Eguchi, R. T., Huyck, C. K., Ghosh, S., and Adams, B. J. (2008). "The application of remote sensing technolo-gies for disaster management," in *14th World Conf on Earthquake Engr* (Beijing), 12–17.

Etkin, D., Brun, S. E., Shabbar, A., and Joe, P. (2001). Tornado climatology of Canada revisited: Tornado activity during different phases of ENSO. *Int. J. Climatol.* 21, 915–938. doi: 10.1002/joc.654

Fleming, M. R., Haan, F. L., and Sarkar, P. P. (2013). "Turbulent structure of tornado boundary layers with translation and surface roughness," in *12th Americas Conf. on Wind Engineering* (Seattle, WA).

Fratinardo, V. F., and Schroeder, S. A. (2013). Accuracy of EF ratings following a tornado event: an engineer's perspective. *Struct. Congress* 2013, 980–990. doi: 10.1061/9780784412848.087

Frelich, L. E., and Ostuno, E. J. (2012). Estimating wind speeds of convective storms from tree damage. *Electro. J. Severe Storms Meteorol.* 7, 1–19.

Fujita, T. T. (1981). Tornadoes and downbursts in the context of generalized planetary scales. *J. Atmos. Sci.* 38, 1511–1534. doi: 10.1175/1520-0469(1981)038<1511:TADITC>2.0.CO;2

Fujita, T. T. (1989). The Teton-Yellowstone tornado of 21 July 1987. *Monthly Weather Rev.* 117, 1913–1940. doi: 10.1175/1520-0493(1989)117<1913:TTYTOJ>2.0.CO;2

Ghosh, S., Huyck, C., Greene, M., Gill, S., Bevington, J., Svekla, W., et al. (2011). Crowdsourcing for rapid damage assessment: the Global Earth Observation Catastrophe Assessment Network (GEO-CAN), *Earthquake Spectra* 27, S179–S198. doi: 10.1193/1.3636416

Glasscoe, M., Parker, J. W., Wang, J., Pierce, M. E., Yoder, M. R., Eguchi, R. T., et al. (2016). "Applications of E-DECIDER decision support tools for disaster response and recovery," in *Applied Geology in California, Association of Environmental and Engineering Geologists (AEEG) Special Publication Number 26*, ed R. Anderson and H. Ferriz (Redwood City, CA: Star Publishing Company), 631–650.

Gneeniss, A. S., Mills, J. P., and Miller, P. E. (2015). In-flight photogrammetric camera calibration and validation via complementary lidar. *ISPRS J. Photogram. Remote Sens.* 100, 3–13. doi: 10.1016/j.isprsjprs.2014.04.019

Godfrey, C., and Peterson, C. (2017). Estimating enhanced fujita scale levels based on forest damage severity. *Weather Forecast.* 32, 243–252. doi: 10.1175/WAF-D-16-0104.1

Gong, J. (2014). "A remote sensing-based approach for assessing and visualizing post-Sandy damage and resiliency rebuilding needs," in *Proc. in Construction Research Congress 2014: Construction in a Global Network*, ASCE (Atlanta, GA), 1259–1268.

Gong, J., and Maher, A. (2014). Use of mobile lidar data to assess hurricane damage and visualize community vulnerability. *Transp. Res. Rec.* 2459, 119–126. doi: 10.3141/2459-14

Graettinger, A. J., Grau, D., J. W., van de Lindt, J., and Prevatt, D. O. (2012). "GIS for the geo-referenced analysis and rapid dissemination of forensic evidence collected in the aftermath of the Tuscaloosa tornado," in *ASCE Const Research Congress*, 2170–2179. doi: 10.1061/9780784412329.218

Graettinger, A. J., Ramseyer, C. E., Freyne, S., Prevatt, D. O., Myers, L., and Alfano, C. (2014). *Tornado Damage Assessment in the Aftermath of the May 20th 2013 Moore Oklahoma Tornado.* Technical Report to National Science Foundation, Arlington, VA.

Haan, F. L., Balarmudu, V. K., and Sarkar, P. P. (2010). Tornado-induced wind loads on a lowrise building. *J. Struct. Eng.* 136, 106–116. doi: 10.1061/(ASCE)ST.1943-541X.0000093

Haan, F. L., Sarkar, P., Prevatt, D., Roueche, D., Graettinger, A., Dao, T. N., et al. (2014). "Using tornado damage surveys to improve laboratory tornado simulations," in *ASCE Structures Congress* (Boston, MA), 1472–1483. doi: 10.1061/9780784413357.130

Hatzikyriakou, A., Lin, N., Gong, J., Xian, S., Hu, X., and Kennedy, A. (2015). Component-based vulnerability analysis for residential structures subjected to storm surge impact from Hurricane Sandy. *Nat. Hazards Rev.* 17:15. doi: 10.1061/(ASCE)NH.1527-6996.0000205

He, M., Zhu, Q., Du, Z., Hu, H., Ding, Y., and Chen, M. (2016). A 3D shape descriptor based on contour clusters for damaged roof detection using airborne LiDAR point clouds. *Remote Sens.* 8, 189–211. doi: 10.3390/rs8030189

Hu, H., Yang, Z., Sarkar, P., and Haan, F. (2011). Characterization of the wind loads and flow fields around a gable-roof building model in tornadolike winds. *Exp. Fluids* 51, 835–851. doi: 10.1007/s00348-011-1102-6

Huang, Z., Fan, X., Liping, C., and Shi, S. Q. (2016). Tornado hazard for structural engineering. *Nat. Hazards* 83, 1–22. doi: 10.1007/s11069-016-2392-z

ImageCat/New Light Technologies (2011). *Rapid Damage Assessment using Remote Sensing Imagery - Tuscaloosa (Alabama), Birmingham (Alabama), Joplin (Missouri). Report to the Federal Emergency Management* Agency.

Jedlovec, G. J., Nair, U., and Haines, S. L. (2006). Detection of storm damage tracks with EOS data. *Weather Forecast.* 21, 249–267. doi: 10.1175/WAF923.1

Jurkofsky, D. (2015). Accuracy of SUAS Photogrammetry for use in accident scene diagramming. *SAE Int. J. Transp. Safety* 3, 136–152. doi: 10.4271/2015-01-1426

Karstens, C. D., Gallus, W. A., Lee, B. D., and Finley, C. A. (2013). Analysis of tornado-induced tree fall using aerial photography from the Joplin, Missouri, and Tuscaloosa-Birmingham, Alabama, tornadoes of 2011. *Appl. Meteorol. J. Climatol.* 52, 1049–1068. doi: 10.1175/JAMC-D-12-0206.1

Karstens, C. D., Samaras, T. M., Lee, B. D., Gallus, W. A., and Finley, C. A. (2010). Near-ground pressure and wind measurements in tornadoes. *Monthly Weather Rev.* 138, 2570–2588. doi: 10.1175/2010MWR3201.1

Kashani, A. G., Crawford, P. S., Biswas, S. K., Graettinger, A. J., and Grau, D. (2015). Automated tornado damage assessment and wind speed estimation based on terrestrial laser scanning. *J. Comput. Civil Eng.* 29, 1–10. doi: 10.1061/(ASCE)CP.1943-5487.0000389

Kashani, A. G., and Graettinger, A. J. (2015). Cluster-based roof covering damage detection in ground-based lidar data. *Autom. Constr.* 58, 19–27. doi: 10.1016/j.autcon.2015.07.007

Kashani, A. G., Graettinger, A. J., and Dao, T. (2014). "3D data collection and automated damage assessment for near real-time tornado loss estimation," in *ASCE Construction Research Congress* (Atlanta, GA), 1209–1218. doi: 10.1061/9780784413517.124

Kashani, A. G., Graettinger, A. J., and Dao, T. (2016). Lidar-based methodology to evaluate fragility models for tornado-induced roof damage. *Nat. Hazards Rev.* 17:3. doi: 10.1061/(ASCE)NH.1527-6996.0000224

Kedzierski, M., and Fryskowska, A. (2015). Methods of laser scanning point clouds integration in precise 3D building modelling. *Measurement* 74, 221–232. doi: 10.1016/j.measurement.2015.07.015

Kijewski-Correa, T., Gong, J., Kennedy, A., Womble, J., A., Cai, C. S., and Wood, R. L. (2018). "Performance of Low-Rise Construction under Wind and Coastal Hazards during the Landfall of Hurricane Harvey," in *ASCE Forensics Congress* (Austin, TX).

Kikitsu, H., and Sarkar, P. P. (2015). Building damage, wind speed estimation, and post disaster recovery in an EF5 tornado. *Nat. Hazards Rev.* 16:04014019. doi: 10.1061/(ASCE)NH.1527-6996.0000156

Kingfield, D., and deBeurs, K. (2014). "On the role of urban and vegetative land cover in the identification of tornado damage using dual-resolution multispectral satellite imagery," in *Proc: American Geophysical Union, Fall Meeting 2014* (San Francisco, CA), #NH11B-3701.

Koliou, M., Masoomi, H., and van de Lindt, J. W. (2017). Performance assessment of tilt-up big-box buildings subjected to extreme hazards: tornadoes and earthquakes. *J. Perform. Constru. Facilit.* 31:04017060. doi: 10.1061/(ASCE)CF.1943-5509.0001059

Kopp, G. A., Hong, E., Gavanski, E., Stedman, D., and Sills, D. M. L. (2017). Assessment of wind speeds based on damage observations from the Angus (Ontario) Tornado of 17 June 2014. *Can. J. Civil Eng.* 44, 37–47. doi: 10.1139/cjce-2016-0232

Kosiba, K., and Wurman, J. (2010). The three dimensional axisymmetric wind field structure of the Spencer, South Dakota, 1998 tornado. *J. Atmos. Sci.* 67, 3074–3083. doi: 10.1175/2010JAS3416.1

Kosiba, K. A., and Wurman, J. (2013). The three-dimensional structure and evolution of a tornado boundary layer. *Weather Forecast.* 28, 1552–1561. doi: 10.1175/WAF-D-13-00070.1

LaDue, J. G., Levitan, M. L., Karstens, C., Lombardo, F. T., MacAloney, B. W., Brown-Giammanco, T. M., et al. (2017). "Poster: progress of the ASCE wind speed estimation standards committee," in *American Meteorological Society Annual Conference* (Seattle, WA).

LaDue, J. G., and Mahoney, E., A. (2006). "Implementing the new enhanced Fujita scale within the NWS," in *23rd Conf on Severe Local Storms* (St. Louis, MO: *Amer. Meteor. Soc*). Available online at: http://ams.confex.com/ams/pdfpapers/115420.pdf

Lee, W. C., and Wurman, J. (2005). Diagnosing new details about tornado dynamics. *Bull. Am. Meteorol. Soc.* 86, 1547–1550.

Lloyd's of London (2013). *Tornadoes: A Rising Risk?* Available online at: http://www.lloyds.com/$\sim$/media/Lloyds/Reports/Emerging-Risk-Reports/Tornadoes-final-report.pdf

Lombardo, F. T., Brown, T. M., Levitan, M. L., and LaDue, J. G. (2015a). "Estimating wind speeds in tornadoes and other windstorms: Development of an ASCE standard," in *14th Intl. Conference on Wind Engineering* (Porto Alegre), 21–26.

Lombardo, F. T., Roueche, D. B., and Prevatt, D. O. (2015b). Comparison of two methods of near-surface wind speed estimation in the 22 May 2011 Joplin, Missouri tornado. *J. Wind Eng. Ind. Aerodyn.* 138, 87–97. doi: 10.1016/j.jweia.2014.12.007

Luo, J., Liang, D., Kafali, C., Li, R., and Brown, T. M. (2014a). Enhanced remote-sensing scale for wind damage assessment. *J. Wind Struct.* 19, 321–337. doi: 10.12989/was.2014.19.3.321

Luo, J., Liang, D., and Weiss, C. (2014b). Reconstruction of a near-surface tornado wind field from observed building damage. *Wind Struct.* 20, 389–404. doi: 10.12989/was.2015.20.3.389

Magsig, M., Dickens-Micozzi, M., and Yuan, M. (2000). "Analysis of tornado damage on May 3rd 1999 using remote sensing and GIS methods on high-resolution satellite imagery," in Proc. *20th Conference on Severe Local Storms* (Orlando, FL: American Meteorological Association), 9–12.

Masoomi, H., and, van de Lindt, J. W. (2016). Tornado fragility and risk assessment of an archetype masonry school building. *Eng. Struct.* 128, 26–43. doi: 10.1016/j.engstruct.2016.09.030

McDonald, J. R. (2001). Theodore Fujita: his contribution to tornado knowledge through damage documentation and the Fujita scale. *Bull. Am. Meteorol. Soc.* 82, 63–72. doi: 10.1175/1520-0477(2001)000<0063:TTFHCT>2.3.CO;2

McDonald, J. R., Mehta, K. C., Smith, D. A., and Womble, J. A. (2009). "The Enhanced Fujita Scale: development and implementation," in *5th Cong. on Forensic Engr* (Washington, DC), 719–728.

Miller, P. C. (2017). May 24. On the spot: Textron, Aeryon assess Oklahoma tornado damage. *UAS Magazine.* Available online at: http://www.uasmagazine.com/articles/1700/on-the-spot-textron-aeryon-assess-oklahoma-tornado-damage (Accessed January 19, 2018).

Mishra, A. R., James, D. L., and Letchford, C. W. (2008). Physical simulation of a single-celled tornado-like vortex, Part B: Wind loading on a cubical model. *J. Wind Eng. Ind. Aerodyn.* 96, 1258–1273. doi: 10.1016/j.jweia.2008.02.063

Mohammadi, M. E., Wood, R. L., Womble, J. A., Smith, D. A., and Louden, E. I. (2017). "Tornado damage preservation via 3D reality capture," in *13th Americas (International) Conference on Wind Engineering* (Gainesville, FL). 21–24.

Molthan, A., Jedlovec, G., and Carcione, B. (2011). NASA satellite data assist in tornado damage assessments. *EOS* 92, 337–339. doi: 10.1029/2011EO400002

Molthan, A. L., Bell, J. R., Cole, T. A., and Burks, J. E. (2014). Satellite-based identification of tornado damage tracks from the 27 April 2011 severe weather outbreak. *J. Oper. Meteorol.* 2, 191–208. doi: 10.15191/nwajom.2014.0216

Moss, R. E. S., Thompson, E. M., Scott Kieffer, D., Tiwari, B., Hashash, Y. M. A., Acharya, I., et al. (2015). Geotechnical effects of the 2015 magnitude 7.8 Gorkha, Nepal, earthquake & aftershocks Seismo. *Res. Lett.* 86, 1514–1523. doi: 10.1785/0220150158

Murphy, R., (2015). *Robots to the Rescue.* Available online at: www.nsf.gov/mobile/discoveries/disc_images.jsp?cntn_id$=$136160&org$=$NSF

Myint, S. W., Yuan, M., Cerveny, R., and Giri, C. P. (2008). Comparison of remote sensing image process-ing techniques to identify tornado damage areas from Landsat TM data. *Sensors* 8, 1128–1156. doi: 10.3390/s8021128

NIST (2014a). *Measurement Science R&D Roadmap for Windstorm and Coastal Inundation Impact Reduction*. Available online at: www.nist.gov/customcf/get_pdf.cfm?pub_id$=$915541 (Accessed Dec, 07,2017).

NIST (2014b). *Technical Investigation of the May 22, 2011, Tornado in Joplin, Missouri*. Final Report, NIST, 428.

Olsen, M. J., Cheung, K. F., Yamazaki, Y., Butcher, S., Garlock, M., Yim, S., et al. (2012). Damage assessment of the 2010 Chile earthquake & tsunami using terrestrial laser scanning. *Earthquake Spectra* 28, S179–S197. doi: 10.1193/1.4000021

Ortega, B., Garfield, K., LaDue, M., Meyer, S., Speheger, and Stumpf (2014). "Damage survey and analysis of the 20 May 2013 Newcastle–Moore EF-5 Tornado," in *Special Symp. on Severe Local Storms*: *The Current State of the Science and Understanding Impacts* (Atlanta, GA: American Meteorological Society), 828. Available online at: https://ams.confex.com/ams/94Annual/webprogram/Paper241554.html

Osman, M., and Tahar, K. N. (2016). 3D accident reconstruction using low-cost imaging technique. *Adv. Eng. Softw.* 100, 231–237. doi: 10.1016/j.advengsoft.2016.07.007

Peng, X., Roueche, D. B., Prevatt, D. O., and Gurely, K. R. (2016). "An engineering-based approach to predict tornado-induced damage," in *Multi-Hazard Approaches to Civil Infrastructure Engineering*, eds P. Gardoni and J. LaFave (Cham: Springer). doi: 10.1007/978-3-319-29713-2

Peterson, C. J. (2003). "Factors influencing treefall risk in tornadoes in natural forests," in *Preprints, Symp. on the F-Scale and Severe- Weather Damage Assessment* (Long Beach, CA: Am. Meteor. Soc), 3.1.

Peterson, C. J. (2007). Consistent influence of tree diameter and species on damage in nine eastern North America tornado blowdowns. *For. Ecol. Manage.* 250, 96–108. doi: 10.1016/j.foreco.2007.03.013

Pittore, M., Wieland, M., and Fleming, K. (2016). Perspectives on global dynamic exposure modeling for geo-risk assessment. *Nat. Hazards* 86, 7–30. doi: 10.1007/s11069-016-2437-3

Prevatt, D. O., Coulbourne, W., Graettinger, A. J., Pei, S., Gupta, R., and Grau, D. (2013). *Joplin, Missouri, Tornado of May 22, 2011: Structural Damage Survey and Case for Tornado-Resilient Building Codes,* ASCE Structural Engineering Institute.

Prevatt, D. O., Roueche, D. B., van de Lindt J. W., Pei, S., Dao, T., Coulbourne, W., et al. (2012b). "Building damage observations and EF classifications from

the Tuscaloosa AL and Joplin MO tornadoes," in *Proc. Struct. Congress* (Reston, VA: ASCE), 999–1010. doi: 10.1061/9780784412367.089

Prevatt, D. O., Van de Lindt J. W., Back, E. W., Graettinger, A. J., Pei, S., Coulbourne, W., et al. (2012a). Making the case for improved structural design: Tornado outbreaks of 2011. *Leadersh. Manage. Eng.* 192, 254–270. doi: 10.1061/(ASCE)LM.1943-5630.0000192

Prevatt, D. O., Van de Lindt J. W., Graettinger, A., Coulbourne, W., Gupta, R., Pei, S., et al. (2011). *Damage Study and Future Direction for Structural Design Following the Tuscaloosa Tornado of 2011*. 56. Availble online at: http://www.strongtie.com/ftp/articles/tuscaloosatornadoreport2011.pdf

PropertyCasualty360 (2013). *Rapid Access Technology Provides Visual Intelligence after a Disaster*. Available online at: http://www.propertycasualty360.com/2013/10/01/rapid-access-technology-provides-visual-intelligen, (Accessed January 27, 2018).

Radhika, S., Tamura, Y., and Matsui, M. (2012). Use of post-storm images for automated tornado-borne debris path identification using texture-wavelet analysis. *J. Wind Eng. Ind. Aerodynam.* 107–108, 202–213. doi: 10.1016/j.jweia.2012.04.016

Radhika, S., Tamura, Y., and Matsui, M. (2015). Cyclone damage detection on building structures from pre- and post-satellite images using wavelet based pattern recognition. *J. Wind Eng. Ind. Aerod.* 136, 23–33. doi: 10.1016/j.jweia.2014.10.018

Ramseyer, C., Holliday, L., and Floyd, R. (2016). Enhanced residential building code for tornado safety. *J. Perform. Constr. Facilit.* 30:04015084. doi: 10.1061/(ASCE)CF.1943-5509.0000832

Roueche, D., and Prevatt, D. O. (2013). Residential damage patterns following the 2011 Tuscaloosa AL, and Joplin MO Tornadoes. *J. Disaster Res.* 8, 1061–1067. doi: 10.20965/jdr.2013.p1061

Roueche, P., Haan, F. L., and Datin, P. L. (2015). An estimate of tornado loads on a wood-frame building using database-assisted design methodology. *J. Wind Eng. Ind. Aerodyn.* 138, 27–35. doi: 10.1016/j.jweia.2014.11.011

Schaefer, J. T., and Galway, J. G. (1982). "Population biases in the tornado climatology," in *12th Conf. Severe Local Storms* (Kansas City, MO: Am. Meteorological Soc), 51–62.

Schultz, L. (2016). *NASA Short-term Prediction Research and Transition Center (SPoRT), Personal Communication*.

Schultz, L. A. (2017). *Detecting Tornado Tracks Using Synthetic Aperture Radar (SAR) Imagery*. Available online at: https://nasasport.wordpress.com/2017/06/05/detecting-tornado-tracks-using-synthetic-aperture-radar-sar-imagery/ (Accessed January 26, 2018).

Sengupta, A., Haan, F. L., Sarkar, P. P., and Balaramudu, V. (2008). Transient loads on buildings in microburst and tornado winds. *J. Wind Eng. Ind. Aerodyn*. 96, 2173–2187. doi: 10.1016/j.jweia.2008.02.050

Sills, D., Cheng, V., McCarthy, P., Rousseau, B., Waller, J., Elliott, L., et al. (2012). "Using tornado, lightning and population data to identify tornado prone areas in Canada," in *Preprints 26th AMS Conf. Severe Local Storms* (Nashville, TN: Am. Met. Soc.), 59.

Sills, D. M. L. (2012). *Tornadoes in Canada-Improving Our Understanding*. London, ON: Institute for Catastrophic Loss Reduction. Available online at: https://www.iclr.org/images/SILLS_ICLR_Final.pdf (Accessed January 7, 2017).

Skow, K. D., and Cogil, C. (2017). High-Resolution aerial survey and radar analysis of quasi-linear convective system surface vortex damage paths from 31 august 2014. *Weather Forecast.* 32, 441–467. doi: 10.1175/WAF-D-16-0136.1

Smith, T. L., Perotin, M., and Walsh, E. (2012). "Enhancing tornado performance of critical facilities: findings and recommendations of FEMA's mitigation assessment team," in *ASCE Structures Congress* (Chicago, IL), 977–988.

Snider, C. R. (1977). A look at Michigan tornado statistics. *Monthly Weather Rev.* 105, 1341–1342.

Stal, C., Tack, F., DeMaeyer, P., DeWulf, A., and Goossens, R. (2013). Airborne photogrammetry and lidar for DSM extraction and 3D change detection over an urban area – a comparative study. *Int. J. Remote Sens.* 34, 1087–1110. doi: 10.1080/01431161.2012.717183

Standohar-Alfano, C. D., and van de Lindt, J. W. (2016). Tornado risk analysis for residential wood frame roof damage across the United States. *J. Struct. Eng.* 142, 1–12. doi: 10.1061/(ASCE)ST.1943-541X.0001353

Szabo, S., Enyedi, P., Horvath, M., Kovacs, A., Burai, P., Csoknyai, T., et al. (2016). Automated registration of potential locations for solar energy production with Light Detection and Ranging (LiDAR) and small format photogrammetry. *J. Cleaner Product.* 112, 3820–3829. doi: 10.1016/j.jclepro.2015.07.117

Thampi, H., Dayal, V., and Sarkar, P. P. (2011). Finite element analysis of interaction of tornados with a low-rise timber building. *J. Wind Eng. Ind. Aerodyn.* 99, 369–377. doi: 10.1016/j.jweia.2011.01.004

Thomas, J., Kareem, A., and Bowyer, K. W. (2014). Automated poststorm damage classification of low-rise building roofing systems using high-resolution aerial imagery, *IEEE Trans. Geosci. Remote Sens.* 52, 3851–3861. doi: 10.1109/TGRS.2013.2277092

Thomas, J., Kareem, A., and Bowyer, K. W., (2012). "Recent advances towards a robust, automated hurricane damage assessment from high-resolution images," *Adv. Hurricane Eng* (Miami, FL: ASCE), 806–815. doi: 10.1061/9780784412626.069

TTU - WiSE, (2006). *A Recommendation for an Enhanced Fujita Scale (EF-Scale)*. Lubbock, TX: Wind Science and Engineering Center, Texas Tech University, 95.

van de Lindt, J. W., Pei, S., Dao, T., Graettinger, A., Prevatt, D. O., Gupta, R., et al. (2013). Dual-objective based tornado design philosophy. *J. Struct. Eng ASCE* 139, 251–263. doi: 10.1061/(ASCE)ST.1943-541X.0000622

van Derostyne, D. A., Hallet, S. K., and Nichols, J. A. (2012). "Post-event forensic investigation of damaged structures from strong wind events," in *Forensic Engineering 2012: Gateway to a Safer Tomorrow, ASCE* (San Francisco, CA), 841–850. doi: 10.1061/9780784412640.089

van Tassel, E. L. (1955). The North Platte Valley tornado outbreak of June 27,1955. *Monthly Weather Rev.* 83, 255–264. doi: 10.1175/1520-0493(1955)083<0255:TNPVTO>2.0.CO;2

Wakimoto, R. M., Atkins, N. T., Butler, K. M., Bluestein, H. B., Thiem, K., Snyder, J. C., et al. (2016). Aerial damage survey of the 2013 El Reno Tornado combined with mobile radar data. *Monthly Weather Rev.* 144, 1749–1775. doi: 10.1175/MWR-D-15-0367.1

Walsh, E., and Tezak, S. (2012). "Findings and Recommendations of FEMA's Mitigation Assessment Team Investigations of the Spring 2011 Tornado Outbreaks," in *Forensic Engineering 2012: Gateway to a Safer Tomorrow*, (San Francisco, CA: ASCE), 821–830. doi: 10.1061/9780784412640.087

Womble, J. A. (2005). *Remote-Sensing Applications to Windstorm Damage Assessment* Doctoral Dissertation, Texas Tech University, Lubbock, TX.

Womble, J. A., Adams, B. J., and Mehta, K., C. (2007a). "Remote Sensing Assessment of Wind Damage," in *MCEER 5th Intl. Workshop on Remote Sensing for Disaster Response* (Washington, DC). Available online at: https://www.gwu.edu/$\sim$spi/assets/docs/Womble-Mehta-Adams%20-%20Remote-Sensing%20Assessment%20of%20Wind%20Damage.pdf

Womble, J. A., Adams, B. J., and Mehta, K. C. (2007b). *Automated Building Damage Assessment Using Remote-Sensing Imagery*. Long Beach, CA: Proc. ASCE Structures Congress.

Womble, J. A., Ghosh, S., Friedland, C. J., and Adams, B. J. (2006). *Hurricane Katrina – Advanced Damage Detection: Integrating Remote-Sensing Images with VIEWSTM Field Reconnaissance.* MCEER Report, Univ. Buffalo.

Womble, J. A., Smith, D. A., Schroeder, J. L., Liang, D., Brown, T. M., and Mehta, K. C. (2010). "Imagery-based wind damage functions," in *Proc. ASCE/SEI Structures Congress* (Orlando, FL), 1099–1108.

Womble, J. A., Wood, R. L., Eguchi, R. T., Ghosh, S., and Mohammadi, M. E. (2016). "Current methods and future advances for rapid, remote-sensing-based wind damage assessment," in *Proc. Resilient Infrastructure: 5th Intl. Natural Disaster Mitigation Spec. Conf.* (London, ON).

Womble, J. A., Wood, R. L., Mohammadi, M. E., Eguchi, R. T., and Ghosh, S. (2017a). "Recent advances in remote-sensing assessments of wind damage," in *13th Americas (International) Conference on Wind Engineering* (Gainesville, FL), 21–24.

Womble, J. A., Wood, R. L., Smith, D. A., Louden, E. I., and Mohammadi, M. E. (2017b). *"Reality Capture for Tornado Damage to Structures*. Denver, CO: ASCE Structures Congress.

Wood, R. L., and Mohammadi, M. E. (2015). *LiDAR Scanning With Supplementary UAV Captured Images for Structural Inspections*. Denver, CO: Intl. LiDAR Mapping Forum, 10.

Wurman, J., Kosiba, K., and Robinson, P. (2013). *In-situ*, Doppler radar, and video observations of the interior structure of a tornado and the wind–damage relationship. *Bull. Am. Meteorol. Soc.* 94, 835–846. doi: 10.1175/BAMS-D-12-00114.1

Wurman, J., Kosiba, K., Robinson, P., and Marshall, T. (2014). The role of multiple-vortex tornado structure in causing storm researcher fatalities, *Bull. Am. Meteorol. Soc.* 95, 31–45. doi: 10.1175/BAMS-D-13-00221.1

Yang, Z., Sarkar, P., and Hu, H. (2011). An experimental study of a high-rise building model in tornado-like winds. *J. Fluids Struct.* 27, 471–486. doi: 10.1016/j.jfluidstructs.2011.02.011

Yuan, M., Dickens-Micozzi, M., and Magsig, M., A. (2002). Analysis of tornado damage tracks from the 3 May tornado outbreak using multispectral satellite imagery. *Weather Forecast.* 17, 382–398. doi: 10.1175/1520-0434(2002)017<0382:AOTDTF>2.0.CO;2

Zhou, Z., Gong, J., and Guo, M., (2016). Image-based 3D reconstruction for posthurricane residential building damage assessment. *J. Comput. Civil Eng.* 30:04015015. doi: 10.1061/(ASCE)CP.1943-5487.0000480

Conflict of Interest Statement: The authors declare that the research was conducted in the absence of any commercial or financial relationships that could be construed as a potential conflict of interest.